HHS Public Access

Author manuscript

Neuroimage. Author manuscript; available in PMC 2019 March 01.

Published in final edited form as:

Neuroimage. 2018 March ; 168: 437–451. doi:10.1016/j.neuroimage.2017.07.003.

Spinal cord MRI at 7T

Robert L. Barry[1,2,*], **S. Johanna Vannesjo**[3], **Samantha By**[4,5], **John C. Gore**[4,5,6], and **Seth A. Smith**[4,5,6]

[1]Athinoula A. Martinos Center for Biomedical Imaging, Department of Radiology, Massachusetts General Hospital, Charlestown, Massachusetts, USA

[2]Department of Radiology, Harvard Medical School, Boston, Massachusetts, USA

[3]Oxford Centre for Functional MRI of the Brain (FMRIB), Nuffield Department of Clinical Neurosciences, University of Oxford, Oxford, UK

[4]Vanderbilt University Institute of Imaging Science, Vanderbilt University Medical Center, Nashville, Tennessee, USA

[5]Department of Biomedical Engineering, Vanderbilt University, Nashville, Tennessee, USA

[6]Department of Radiology and Radiological Sciences, Vanderbilt University Medical Center, Nashville, Tennessee, USA

Abstract

Magnetic resonance imaging (MRI) of the human spinal cord at 7 Tesla has been demonstrated by a handful of research sites worldwide, and the spinal cord remains one of the areas in which higher fields and resolution could have high impact. The small diameter of the cord (~1 cm) necessitates high spatial resolution to minimize partial volume effects between gray and white matter, and so MRI of the cord can greatly benefit from increased signal-to-noise ratio and contrasts at ultra-high field (UHF). Herein we review the current state of UHF spinal cord imaging. Technical challenges to successful UHF spinal cord MRI include radiofrequency (B_1) nonuniformities and a general lack of optimized radiofrequency coils, amplified physiological noise, and an absence of methods for robust B_0 shimming along the cord to mitigate image distortions and signal losses. Numerous solutions to address these challenges have been and are continuing to be explored, and include novel approaches for signal excitation and acquisition, dynamic shimming and specialized shim coils, and acquisitions with increased coverage or optimal slice angulations.

[*]Address correspondence to: Robert L. Barry, Ph.D., Athinoula A. Martinos Center for Biomedical Imaging, 149 13th Street, Suite 2.301, Charlestown MA 02129, USA, Tel: 615-801-0795, Robert.Barry@mgh.Harvard.edu.

Conflict of Interest

The authors declare no conflict of interest.

INTRODUCTION

Magnetic resonance imaging (MRI) of the human spinal cord has been a routine clinical procedure since the 1980s, and for roughly two decades, spinal cord examinations were commonly performed at a clinical field strength of 1.5 Tesla. Within the last decade, however, 3 Tesla scanners have been widely adopted for spinal cord imaging. The advantages of MRI at 3T vs. 1.5T are a theoretical doubling of the signal-to-noise ratio (SNR) (Edelstein et al., 1986), which can translate into higher spatial resolutions and/or faster exam times, and different field-strength dependent contrasts. For these reasons, spinal cord MRI at 3T has quickly become the standard in both clinical and research settings.

The past decade and a half has also seen a steady growth in the use of even higher fields. Scanners operating at 4 Tesla were developed even before 3T systems were commonplace (Uğurbil, 2012), but more recently MRI scanners operating at ultra-high field (UHF) — defined herein to be 7 Tesla and above — have created new and exciting opportunities for high-resolution imaging. UHF MRI in humans was first reported at 8 Tesla in 1998 (Robitaille et al., 1998), and functional magnetic resonance imaging (fMRI) has been performed in the human brain at 7T since the turn of the century (Yacoub et al., 2001). Approximately 60 UHF systems for human imaging are now installed or planned worldwide. UHF MRI generates exquisite images of the brain with unique contrasts at high spatial resolutions, and UHF fMRI offers higher sensitivity to blood oxygenation level dependent (BOLD) signal changes at higher spatial resolutions (Uğurbil, 2012; Duyn, 2012). However, whereas technologies for MRI of the brain at 7T have advanced significantly within the past 15 years, developments in spinal cord MRI at 7T have lagged considerably and only within recent years have studies been reported that demonstrate the feasibility of structural, functional, quantitative, and spectroscopic imaging in the human spinal cord at 7T.

The last 15+ years of 7T MRI and fMRI in the brain have also produced considerable evidence that methods developed for routine imaging at conventional fields do not readily, if at all, translate to 7 Tesla. Each increase in field strength, from 1.5T to 3T, and from 3T to 7T, offers new opportunities to visualize structures of interest with high spatial resolution and enhanced conspicuity, and to detect brain function and networks with greater sensitivity. However, higher magnetic fields also incur significant technical challenges related to both physics and physiological limitations that must be overcome to fully exploit the theoretical advantages of UHF imaging. Thankfully, new challenges at each field strength increment have also been met with increasingly clever technical solutions (Webb & Van de Moortele, 2016), thereby continually redefining the boundaries of what is practical and what may be possible in the future. Thus, the goals of this review are to present the current state of spinal cord MRI at 7T, explore technical challenges that are currently being addressed by research groups worldwide, and highlight ideas that may advance the frontier of UHF spinal cord imaging.

LITERATURE OVERVIEW

An in-depth literature search was performed through PubMed and the proceedings of the International Society for Magnetic Resonance in Medicine (ISMRM) to identify as many 7T spinal cord publications as possible. Keyword searches included terms such as “spine” and “spinal cord”, and author lists and references within abstracts were cross-referenced through PubMed to obtain the corresponding journal articles, whenever possible. One abstract was also identified in the proceedings of the European Society for Magnetic Resonance in Medicine and Biology. The resultant findings, representing the history and current state of spinal cord MRI at 7T, are presented in Table 1. Any omissions in this table, other than papers that became “in press” between when this manuscript was completed in March 2017 and when it was published online, are inadvertent. All peer-reviewed journal publications are preceded by ISMRM abstracts, but not all abstracts resulted in journal publications, so this list is sorted in chronological order where date of online journal publication supersedes date of first presentation at a conference (with both dates listed). For ISMRM abstracts that were also published as journal articles, the median time between first presentation of the research at ISMRM (taken to be the first day of scientific sessions) and online journal publication is 361 days, with a minimum of −160 days (the journal article was published online a few days after the ISMRM abstract submission deadline) and a maximum of 1541 days (4.2 years).

Table 1 presents 39 unique investigations (18 abstracts and 21 peer-reviewed journal articles) on imaging the human spine or spinal cord at 7T. This list also includes population cohorts, 7T vendor, spine region imaged, and the coils used to acquire data. Of these 39 studies: 1 is *in silico*, 1 is *ex vivo*, 3 only scanned phantoms, and 34 are *in vivo*. Of the 38 studies that acquired data on a 7T scanner (i.e., excluding *in silico*): 1 used Magnex, 2 used GE, 12 used Philips, and 23 used Siemens. Of the 34 *in vivo* studies: 26 exclusively scanned healthy volunteers and 8 included cohorts of patients. Of the 8 patient cohorts: 1 was scoliosis (2 patients), 1 was spina bifida (1 patient), 1 was amyotrophic lateral sclerosis (1 patient), 1 was spinal cord injury (1 patient), and 4 were multiple sclerosis (20, 15, 2, and 10 patients, respectively). Of the 34 *in vivo* studies: 2 imaged the lumbar cord, 4 imaged the thoracic cord, 6 imaged a combination of two or more segments (thoracolumbar, cervicothoracolumbar, or cervicothoracolumbosacral), and 22 imaged the cervical cord (including one that imaged the brain and cervical cord). The geographical locations of the 7T sites that produced these studies are: 1 in France (Marseille), 2 in The United Kingdom (Oxford), 5 in The Netherlands (2 in Leiden, 3 in Utrecht), 5 in Germany (1 in Berlin, 4 in Essen), and 26 in The United States of America (1 in Minneapolis, MN; 1 in Pittsburgh, PA; 1 in Philadelphia, PA; 1 in Mayfield, OH; 2 in San Francisco, CA; 3 in Bethesda, MD; 4 in Boston, MA; 6 in New York, NY; and 7 in Nashville, TN). Finally, the recent growth in this field is evident in the fact that more than half of these 7T references have been published within the last two years.

TECHNICAL CHALLENGES AND DEVELOPMENTS

The potential benefits of UHF spinal cord MRI over established 3T protocols has recently been demonstrated (Figure 1). However, there are still considerable technical challenges

associated with 7T spinal cord imaging to overcome — most notably related to transmit and receive B_1 fields, specific absorption rate (SAR), B_0 inhomogeneities and physiological noise. Addressing these issues will necessitate unique and innovative technical solutions. Certain technologies that were originally developed for imaging the brain *may be* translatable to the cervical or thoracolumbar cord. Similarly, other approaches that are being implemented in spinal cord MRI at 3T (Cohen-Adad & Wheeler-Kingshott (eds.), 2014; Cohen-Adad, 2017) *may be* extended to 7T. In this section we outline the most significant challenges encountered, and discuss current and future directions of development.

Coil Design & B_1 Field

An important observation about Table 1 is that more than half of the studies (20 of 39) are entirely on coil design or involve an aspect of coil design. This makes sense because the quality of the MR data is fundamentally limited by the radiofrequency (RF) coils used for signal excitation and reception, and expectedly, variations in coil design can drastically change radiofrequency (i.e., B_1) field patterns. The optimal coil configuration for 7T spinal cord imaging is not yet known and the brief descriptions of RF coils in Table 1 demonstrate the wide range of ideas for both signal excitation and reception, including both in-house solutions and commercial products. Figure 2 illustrates the wide range of 7T spine coils that have been developed and/or are being used across 7T sites.

There are several technical challenges with spinal cord coil design at 7T. As with all anatomies at 7T, the short electromagnetic wavelengths associated with high fields compromise B_1 homogeneity. Further exacerbating the B_1 nonuniformities is the presence of vertebral bodies around the spinal cord, which differ in electrical permittivity to surrounding tissue. Due to the B_1 nonuniformities, a whole-body volume coil, as typically used at lower field strengths, is generally unsuitable at UHF, and the use of multiple transmit elements has been proposed. With multiple transmit coils, RF shimming can be employed to optimize the phase and amplitude of each transmit element to create a more homogenous B_1^+ field (e.g., Mao et al., 2006; Curtis et al., 2012). Several groups have implemented such a design in the form of transceiver arrays, combining transmit and receive elements, with up to 8 channels employed (Kraff et al., 2009; Sigmund et al., 2012; Wu et al., 2010).

Other groups, however, have taken a different approach and separated transmit and receive components from one another (Vossen et al., 2011; Zhao et al., 2014; Zheng et al., 2016). While some of these designs still implement more than one transmit channel, these coil systems primarily take advantage of the higher number of receive channels, which are more readily available. The increased number of receive channels addresses other technical challenges of coil design for spinal cord imaging: (1) a large field of view (FOV) can be achieved, in order to image several levels of the spinal cord and (2) deep B_1^- penetration is facilitated, which is necessary as the spine is located near the center of the body. While most of the coils (for both configurations) consist of rigid arrays on the posterior side of the neck, it has been shown that contouring individual elements to the spine and/or designing a close-fitting coil former are possible and beneficial (Zhang et al., 2017; Zhao et al., 2014; Yu et al., 2016). Estimated *in vivo* B_1^+ maps have been published for a range of coil configurations: a stripline and loop array (Kraff et al., 2011), dipole arrays (Eryaman et al.,

2015; Duan et al., 2015), a 6-channel wrap-around array (Yu et al., 2016), a 22-channel wrap-around array (Zhang et al., 2017), and a coaxial waveguide (Andreychenko et al., 2013).

It is important to note that increasing the number of coil elements, however, increases the SNR at the periphery, and not necessarily at the center of the region of interest. A simulation study suggests that more designs should be explored, introducing the concept of intentional inefficient spin excitation using loop arrays with electric dipole elements to reduce local SAR (Eryaman et al., 2015). Other interesting designs involving traveling waves for the whole body (Andreychenko et al., 2013), dipoles (Duan et al., 2015, 2016; Ali Haghnejad et al., 2015), and a dielectric waveguide and dipole antenna transmit coil (Henning et al., 2016) have also been investigated. Such 7T coil designs are diverse, and reflect the genuine creativity that is needed to advance the field of UHF spinal cord imaging. Furthermore, it should be noted that most of the work on coil design has been solely for the cervical spinal cord. Designing a 7T coil to image the cervical cord is dissimilar from designing a coil to image the thoracolumbar cord due to substantial differences in anatomy at these segments. In addition to the variable length of the cord, the lumbar cord is smaller than the cervical cord, and is surrounded by larger vertebrae and more tissue, which make the lumbar cord less accessible. Furthermore, the required FOV varies for the different segments (neck vs. torso and abdomen). Two groups have shown full spine coverage by acquiring a multi-station scan and repositioning the transmit coil to each station (Vossen et al., 2011) or by using a modular configuration along the spine (Graessl et al., 2014). These methods, while demonstrating the potential and feasibility of full spine coverage at 7T, are not optimized and represent a future research area to explore. The design and validation of a 7T neurovascular coil is also being considered (Ali Haghnejad et al., 2015), which will be needed for simultaneous UHF brain and cervical cord imaging.

Additional topics of interest that relate to the design of UHF spine coils, but have not yet been explored/published in the spinal cord at 7T, include: RF coils for imaging of other nuclei (e.g., ^{23}Na, ^{31}P); modulating the B_1^+ field with high permittivity materials (Haines et al., 2010; Teeuwisse et al., 2012; O'Reilly et al., 2016), which has been demonstrated in the spinal cord at 3T (Yang et al., 2013) but not at higher fields; and imaging with plasma-based transmit coils (Webb & Aussenhofer, 2015). Lastly, as parallel transmit technologies continue to advance at 7T, novel design frameworks, such as array compression networks (Cao et al., 2016; Yan et al., 2016), should be investigated for spinal cord imaging in order to implement a high number of transmit channels more cost-effectively on a system with fewer transmit channels.

Power Deposition

A major challenge for all UHF experiments, brain and spinal cord alike, is that the SAR — the amount of RF power absorbed by tissue per unit time (W/kg) — scales as a function of the square of the main magnetic field (B_0). Therefore, increasing the magnetic field from 3T to 7T results in a greater-than fivefold SAR increase for a given pulse sequence. Guidelines have been established that set acceptable SAR limits (ICNIRP, 1998) and must be considered during sequence development. These limits are hard-coded into scanner software,

so SAR must be reduced by modifying pulse sequences to have lower flip angles and/or a longer repetition time (TR). Such modifications will invariably affect image contrast and scan duration, so many 3T sequences with high peak RF power (e.g., magnetization transfer) or 180° refocusing pulses (e.g., fast spin-echo imaging) are not readily translatable to 7T.

B_0 Shimming

A further major challenge encountered in UHF spinal cord imaging is the presence of severe B_0 field inhomogeneities. Originating from differences in magnetic susceptibility between different tissue types and surroundings, the field distortions scale with the strength of the background field and are therefore a particular concern at UHF. B_0 field distortions interfere with encoding of contrast and spatial origin of the MR signal, commonly causing artifacts in the form of signal loss and geometric distortion, but can also contribute to ghosting, blurring and distorted excitation volumes, amongst other effects.

The largest B_0 field distortions occur around interfaces between tissue and air, which have a susceptibility difference of about 9 ppm (magnetic volume susceptibility χ_{air} = 0.36 ppm, $\chi_{soft\ tissue}$ = −9.05 ppm) (Schenck, 1996). When imaging the spine, this particularly concerns the shape of the neck, thorax and lungs, which all influence the field profile over the spinal column. To a lesser degree, different tissue types also exhibit susceptibility differences, specifically between bone and water-based soft tissue, which differ by about 0.2 ppm (χ_{bone} = −8.86 ppm) (Schenck, 1996). Despite the lower susceptibility difference, the latter is of major significance in spinal cord imaging because it causes highly localized field gradients around the intervertebral junctions.

Static B_0 field homogeneity can be improved by B_0 shimming, i.e., by applying external fields that approximate and counteract local field distortions. Standardly, B_0 shimming is performed with a set of coils designed to produce spherical harmonic fields of up to 2^{nd} or 3^{rd} order. The current through each coil is adjusted on an individual subject basis to optimize field homogeneity within a defined region of interest based either upon an acquired B_0 field map or a set of projections in different orientations (Gruetter, 1993). With a low number of spherical harmonic field terms, it is however not possible to achieve a homogenous field within the whole spine. Generally, the spherical harmonic approximation of the local field holds better for smaller volumes. In spinal cord imaging, the defined shim region should therefore preferably be limited to cover the spinal canal and a limited FOV in the foot-head direction. However, with a small shim volume, care must be taken not to cause excessive field degeneration outside it, which may interfere with e.g. excitation profiles, spatial encoding and fat suppression.

Figure 3 shows the measured field in the cervical region in one subject before and after 2^{nd} order B_0 shimming (Fig. 3B and Fig. 3C, respectively). B_0 shimming counteracts the field distortions induced by the curvature of the neck, reducing the range of field offsets inside the spinal cord within the shim volume from almost 400 Hz to less than 50 Hz. Outside the shim volume, however, the field homogeneity is substantially deteriorated, and extending the shim volume further to cover more segments of the spinal cord would have come at the cost of reduced field homogeneity inside it. Moreover, upon close inspection, the shimmed field map reveals considerable remaining local field distortions at each intervertebral junction,

which are sufficient to cause substantial signal loss due to dephasing in gradient-echo imaging with long echo times. B_0 shimming up to 3rd order or higher could improve field homogeneity over a larger region, but the localized gradients at the intervertebral junctions would persist.

A further challenge of 7T spinal cord B_0 shimming is poor robustness of shim calculation procedures. This is demonstrated for an fMRI scan in Figure 4, where two consecutive scans with identical acquisition parameters and shim regions yielded substantially different shim settings by the standard projection-based vendor-provided shimming procedure. A few factors that likely contribute to this phenomenon can be identified. Primarily, the fit of higher-order field terms is increasingly ill-conditioned for smaller shim volumes, and the shim calculation is therefore more prone to be disturbed by noise and spurious signal (Nassirpour et al., 2017). Under these circumstances, low SNR regions or physiologically induced field fluctuations can substantially influence calculated shim settings. Furthermore, compensating for strong local field gradients can require currents exceeding amplitude limits of the shim coils, in which case the settings may be capped at a suboptimal value. The optimization algorithm should ideally take shim amplitude limits into account, but in practice this is not always the case. The shim calculation should also account for the actual field profiles produced by the shim coils, instead of assuming perfect spherical harmonic shim fields (Webb & Macovski, 1991).

In essence, B_0 shimming of the spinal cord at UHF presently suffers from (1) being feasible for only limited FOVs, (2) an inability to compensate for highly localized field distortions at intervertebral junctions, and (3) poor reproducibility. To overcome these limitations, it will be imperative to take advantage of, and expand upon, recent developments within the area of B_0 shimming. Some benefit may be gained already from simple measures, such as field-map based B_0 shimming with regularized shim calculation (Kim et al., 2002), weighted regions of interest, or prior knowledge of expected shim values for the specific anatomy, whereas further improvement will require more advanced technical solutions.

In UHF brain imaging, it has been proposed to optimize shim settings on a slice-by-slice basis (Blamire et al., 1996; de Graaf et al., 2003; Zhao et al., 2005; Juchem et al., 2010; Sengupta et al., 2011), and a similar approach for axial acquisitions of the spinal cord holds potential to reduce the impact of field inhomogeneities at the intervertebral junctions. A study at 3T demonstrated reduced through-plane dephasing by adding slice-specific Z gradient moments, thereby improving T_2*-weighted echo planar imaging (EPI) acquisitions in the spinal cord (Finsterbusch et al., 2012). Dynamic shim usage could also be instrumental for imaging of extended regions, such as different segments of the cord or simultaneous imaging of the spinal cord and the brain (Finsterbusch et al., 2013). Operating the shims dynamically is relatively straightforward for the first-order terms (i.e., gradients), whereas higher-order shim terms generally require specialized hardware and careful calibration of eddy current compensation (Koch et al., 2006; Juchem et al., 2010; Fillmer et al., 2016; Vannesjo et al., 2017).

Another recent development for B_0 shimming of the brain is the usage of arrays of small shim coils placed in close proximity to the subject (Han et al., 2013; Juchem et al., 2011).

This yields increased degrees of freedom in the achievable shim field profiles, and has been shown to improve field homogeneity in the brain at 7T (Juchem et al., 2011). In this direction, a 24-channel planar shim coil placed in the patient table was recently reported to substantially improve static shimming of the spinal cord at 3T (Topfer et al., 2016).

Finally, passive B_0 shimming has the potential of yielding even higher degrees of freedom in the produced field patterns, however at the expense of being more difficult to adjust on a subject-by-subject basis. For brain imaging, studies have shown field homogeneity improvements by positioning materials with suitably chosen magnetic susceptibility in the vicinity of the subject (Yang et al., 2011), or in the oral cavity (Wilson et al., 2002). For spinal cord imaging at 3T, one study has demonstrated improved field homogeneity within the neck by placing pyrolytic graphite foam matched to the susceptibility of human tissue behind the neck (Lee et al., 2015).

Physiological Noise

Another major consideration of *in vivo* spinal cord imaging at 7T is physiological noise. In its broadest sense, physiological noise refers to any and all physiological processes (respiration, cardiac pulsatility/movement, swallowing, cerebrospinal fluid (CSF) flow, and bulk movement) that create unwanted instabilities in the MR signal. Owing to the slow time scales of the most common sources, physiological noise creates data inconsistencies between RF excitations. These inconsistencies, in turn, manifest in one or more complex ways including (but not limited to): decreased spatial resolution (blurring), image duplication (ghosting), image distortion and loss of desired contrast, suboptimal B_0 shimming and resonance frequency selection, and decreased SNR or functional contrast-to-noise ratio. In multi-shot acquisitions, such as line-byline readouts or segmented EPI, ghosting artifacts and blurring frequently dominate, while single-shot EPI data additionally suffers from variable geometric translations and distortions. Temporally varying instabilities make applications such as high-resolution diffusion tensor imaging and fMRI notoriously challenging in the spinal cord at 7T.

Most physiological noise sources relate to either motion within the imaging volume itself (e.g., CSF flow and pulsatile motion of the spinal cord) or motion outside of the imaging volume (e.g., respiration). The latter affects the MR signal via induced B_0 field changes, due to changed distribution of magnetic susceptibility (Raj et al., 2001). While motion of the tissue itself is independent of field strength, the ensuing B_0 field variations scale with the background field. Most significant are periodic field fluctuations due to respiration, but swallowing or speaking (Birn et al., 1998) and bulk motion (Barry et al., 2010; Versluis et al., 2012) also contribute to the detrimental effects. Due to the close proximity to the lungs, the respiratory-induced field variations are considerably higher throughout the spine than in the brain. Measurements of the cervical and upper thoracic spinal cord at 3T have demonstrated a peak-to-peak field shift of around 74 Hz due to respiration at C7 (Verma & Cohen-Adad, 2014), while recent preliminary reports at 7T indicate shifts of ~140 Hz (Vannesjo et al., 2016) or higher (Pennell et al., 2014) at C7. In comparison, respiratory-related field shifts in the brain at 7T have been reported to be up to around 7 Hz during deep breathing (Duerst et al., 2016).

In fMRI in the brain, sources of physiological noise related to respiration, cardiac pulsatility, and manifestation of the BOLD effect have been characterized at 1.5T (Krüger et al., 2001), 3T (Krüger & Glover, 2001), and 7T (Triantafyllou et al., 2005). Importantly, physiological noise is the dominant noise source at UHF (Triantafyllou et al., 2005) and must be adequately addressed for research to benefit from the gains in BOLD contrast-to-noise ratio at high fields. Various approaches have been proposed to mitigate the impact of physiological noise, including higher resolution acquisitions to reduce the relative influence of unwanted signal fluctuations (Triantafyllou et al., 2006) and, more commonly, the use of one or more post-processing algorithms to model and remove variance related to physiological noise (e.g., RETROICOR, Glover et al., 2000). A current review paper presents a thorough overview of the various approaches to denoise spinal cord fMRI data (Eippert et al., 2017).

As new RF coils become available, future studies can more completely characterize aspects of 7T physiological noise along the entire cord. It is likely that physiological noise will differ considerably between the cervical, thoracic, and lumbar regions. Although all regions of the cord will be affected by respiration, the cervical cord will be more susceptible to swallowing artifacts, the upper thoracic cord will be more susceptible to cardiac motion, and the lower thoracic and lumbar cord will be more susceptible to peristalsis.

Given the multitude of physiological noise sources, and magnitude of their impact, there is an urgent need for developments aimed at reducing physiological noise to realize the full potential of UHF spinal cord imaging. A generic way of addressing physiological noise of cardiac or respiratory origin is to acquire data with gating or triggering based on physiological monitors (e.g., respiratory bellows, electrocardiogram (ECG), pulse oximeter or navigators). At lower field strengths, cardiac triggering is commonly based upon ECG recordings. However, ECG pulse detection is increasingly unreliable at higher field strength due to field-dependent artifact sources, such as magneto-hydrodynamic effects and electromagnetic interferences, and alternative cardiac monitoring techniques are being investigated (Niendorf et al., 2010).

A common drawback of gating and triggering approaches is that they often come at the expense of prolonged scan time and/or additional corrections for T_1 modulation. An alternative approach to deal with physiological noise is to measure and correct for the effects. For brain imaging at UHF, it has been proposed to measure the B_0 field fluctuations induced by respiration with the use of navigators (Versluis et al., 2012), external field sensors (Duerst et al., 2015), or a field model coupled to the trace of respiratory bellows (van Gelderen et al., 2007). The measurements can then be used either for retrospective data correction, for example by incorporation into image reconstruction (Versluis et al., 2012; Vannesjo et al., 2015), or prospective correction by adding compensatory shim fields in real-time (van Gelderen et al., 2007; Duerst et al., 2015). With appropriate adjustments, each of these techniques could potentially be translated to spinal cord imaging. Basic navigator echoes are already being used for UHF spinal cord imaging to reduce phase inconsistencies between shots (Zhao et al., 2014), but it is important to note that navigators techniques originally designed and optimized for the brain may not initially work as intended in the spinal cord. Thus, additional work may be required to re-optimize techniques such as

navigator echo corrections for UHF spinal cord imaging. Finally, UHF spectroscopy in the spinal cord (Henning et al., 2016) can benefit from a “metabolite cycling” technique that performs frequency alignment and phase corrections to compensate for respiratory-induced physiological noise in low SNR spectra (Hock et al., 2013).

Anatomical Considerations

Adding to the previously described predominantly technical issues, there are challenges directly related to the specific anatomical dimensions of the spinal cord, making it inherently challenging to image at any field strength. The small cross-sectional area of the spinal cord (10–12 mm left-right and 8–10 mm anterior-posterior, or *smaller*) necessitates high in-plane resolutions (ideally ~0.5×0.5 mm^2) to minimize partial volume effects, while the elongated shape demands a large FOV in the foot-head direction. Furthermore, the often curved geometry of the spinal cord makes it difficult to implement the directionally-dependent demands on resolution and FOV consistently over all segments. Several techniques developed at lower field strengths will be crucial in the development of imaging protocols that are optimized for the shape of the spinal cord, but many of these techniqes still remain to be translated to UHF and/or adapted for the unique criteria of spinal cord imaging. Examples of techniques with high potential to improve UHF spinal cord imaging are outlined in the following paragraphs.

Due to the small radius of the spinal cord, approaches to reduce the FOV in the transverse plane would be beneficial to accelerate acquisitions and reduce susceptibility-induced distortions. At 3T, reduced FOV imaging of the spinal cord has been implemented using spin-echo acquisitions with tilted refocusing pulses (Wheeler-Kingshott et al., 2002) and/or additional RF pulses for outer volume suppression (Wilm et al., 2009). Both techniques could potentially be translated to 7T, although SAR limitations may restrict the applicability. Alternatively, recent advances in 2D RF pulse design have led to an interesting demonstration at 3T of fMRI in focally excited brain regions at high temporal resolution (Finsterbusch, 2015). It is intriguing to consider that this technique could be applied to the spinal cord at 7T, but 2D pulse design will be challenging to implement at UHF because the long excitation pulses will increase the degree of T_2* relaxation, thereby decreasing SNR, and push the boundaries of SAR limits. However, parallel transmit technologies are continually advancing at 7T (Padormo et al., 2016) and may eventually enable robust 2D RF excitation in the spinal cord.

Another innovative technique that can be translated to the spinal cord is simultaneous multislice (SMS) imaging. SMS was first demonstrated in the human leg (ironically, using a spine coil) in 2001 (Larkman et al., 2001), and has generated tremendous interest in the brain in recent years (e.g., Moeller et al., 2010; Feinberg et al, 2010; Setsompop et al., 2012; Feinberg & Setsompop, 2013; Barth et al., 2016). Acquiring multiple slices simultaneously is particularly intriguing for the spinal cord because, unlike the brain, its extent in the superior-inferior dimension is an order of magnitude greater than the other two dimensions. Figure 5A shows how SMS was employed at 3T to achieve greater coverage for a diffusion tensor imaging (DTI) scan. In the same acquisition time, the non-SMS acquisition (Fig. 5A, left panel) covered 14 slices from C2 to C5, whereas the SMS acquisition (Fig. 5A, right

panel) achieved 30 slices to cover the cervical cord and brainstem. The integration of SMS into cervical spinal cord protocols has already begun at 3T (By et al., 2016), as well as a hybrid approach for brain and spinal cord imaging at 3T (Finsterbusch, 2016), thus similar translations to 7T are anticipated once the various technical challenges (e.g., SAR) can be adequately addressed.

A conundrum inherent in spinal cord imaging is the desire to acquire many axial slices along a structure that curves. Axial acquisitions of the cord have a relatively high in-plane resolution (< 1×1 mm^2, and ideally ~0.5×0.5 mm^2) to minimize within-plane partial volume effects, and relatively thick slices (3–5 mm) to increase SNR and coverage. However, it should be noted that this is only effective if all slices are actually perpendicular to the spinal cord. Otherwise, remaining partial volume effects, particularly between gray and white matter, result in a loss of spatial resolution by blurring adjacent structures. Achieving approximate perpendicularity is occasionally possible when subjects have a remarkably straight spinal cord while positioned in the scanner (Fig. 5B, left panel), but the vast majority of subjects have some degree of natural spinal cord curvature (Fig. 5B, center panel). Therefore, a preferable acquisition strategy would have variable slice angulations to maintain true perpendicularity to the cord from one slice to the next (Fig. 5B, right panel). Slice angulations could be manually set, but ideally the angle for each slice would be set automatically using an algorithm that identifies the curvature of the spinal cord in the sagittal plane (De Leener et al., 2014).

Another area of innovative research at 3T is simultaneous brain and spinal cord imaging (Cohen-Adad et al., 2010; Finsterbusch et al., 2013). This endeavor is very technically challenging due to the different fields of view, required spatial resolutions, optimal shim settings, and locations of receive coils. Despite these challenges, simultaneous BOLD fMRI in the brain and cord is necessary to enable new investigations of task-based sensory/motor processing throughout the cerebrum and spinal cord, and shed new light on the nature of resting state networks within the brain (Biswal et al., 1995, 2010), cerebellum (Buckner et al., 2011), and spinal cord (Barry et al., 2014; Kong et al., 2014; San Emeterio Nateras et al., 2016; Liu et al., 2016) by considering these networks from an integrative perspective of central nervous system function. Simultaneous brain and spinal cord imaging has not yet been demonstrated at 7T, but a recent RF coil design (Ali Haghnejad et al., 2015) suggests that this feat will occur in the near future.

Finally, whereas neuroimaging studies in the brain have benefited from the widespread adoption of standardized atlases and coordinate systems (i.e., Talairach or Montreal Neurological Institute (MNI) space) for decades, the absence of a universally-adopted template and coordinate system for the spinal cord has stunted growth in this field and hindered potential collaboration between sites. However, the *de novo* MNI-Poly-AMU template (Fonov et al., 2014) and spinal cord toolbox (De Leener et al., 2017) have recently been proposed, and these advancements may be widely adopted to faciliate forthcoming developments in spinal cord imaging across field strengths. It should also be noted, however, that spinal cord post-processing methods have typically been developed and validated at 3T, so additional validations may be required to ensure that tools developed at clinical fields also

work robustly at UHF (e.g., due to changes in image resolution, spatial contrasts, and manifestation of artifacts).

Summary

The preceding sections have presented many of the challenges faced by UHF spinal cord imagers. Several ideas that may soon become active areas of UHF research have been presented, but this discussion is by no means exhaustive. Other challenges related to UHF quantitative imaging in the spinal cord, specifically magnetization transfer (MT) and chemical exchange saturation transfer (CEST), have been previously discussed in detail (Smith et al., 2014). Overall, UHF challenges are mainly technical in nature, and, as shown in Table 1, are currently being tackled by various groups worldwide. However, none of these challenges are close to being solved, and collaborative efforts between research groups — and between research sites and their respective 7T vendor — will be required to fully address the many technical difficulties associated with UHF spinal cord imaging.

SEQUENCES IMPLEMENTATIONS

A largely practical, but nonetheless limiting, hurdle in UHF spinal cord imaging is the lack of well-functioning standardized imaging protocols. For brain imaging, there is a large body of published literature to draw upon, and vendors commonly provide optimized protocols for basic applications such as T_1, T_2 or T_2*-weighted imaging, diffusion and fMRI. The same protocols, however, rarely perform to satisfaction in the spinal cord, and optimal sequence parameters for corresponding imaging applications in the spine remain largely unexplored.

Truly optimized protocols will need to take the anatomy and environment of the spine into account, specifically the thin elongated shape of the spinal cord, combined with the local B_0 and B_1 field inhomogeneities, as well as sources of physiological noise. Several acquisition parameters can be tuned to optimize for one factor, albeit frequently as a trade-off against other relevant factors. For example, a shorter echo time (TE) in gradient-echo acquisitions reduces signal dropout, but may also decrease T_2* contrast; increasing acquisition bandwidth reduces geometric distortion, however at a cost of lower SNR; spin echo acquisitions are robust towards dephasing, but are limited by SAR constraints; and multi-shot readouts are less sensitive to B_0 inhomogeneities but more sensitive to motion and physiological noise. For these reasons, 7T spinal cord protocols have thus far gravitated toward gradient-echo acquisitions with short TE. Spatial contrast may be further enhanced through multi-echo image recombination, although care must be taken to ensure that later echoes are not corrupted by cumulative ΔB_0 phase errors.

We refer to the references listed in Table 1 for a complete overview of 7T spinal cord sequence implementations. Of the 26 studies (conference abstract or journal article) that present results from one or more modalities (i.e., excluding exclusive RF coil construction, B_0 field mapping, and algorithm validation): 17 included results on anatomical imaging, 4 on fMRI, 3 on diffusion (2 *in vivo* and 1 *ex vivo*), 2 on CEST, 1 on MT, 1 on parametric mapping, and 1 on spectroscopy. Nearly all anatomical imaging studies included gradient echo images because T_2*-weighted images provide excellent gray/white matter contrast (Figure 1) and visualization of pathologies (Cohen-Adad et al., 2013, 2012; Dula et al.,

2016a). As an example, the first demonstration of high-resolution anatomical imaging was performed using a gradient-echo sequence with an in-plane resolution of 0.18×0.18 mm^2 and 3-mm thick slices (0.097 mm^3 voxels; TE = 4.91 ms; acquisition time = 5 mins 14 sec), taking advantage of a 3.5-fold SNR increase in the cervical cord using a specialized 7T coil vs. a standard 3T coil (Sigmund et al., 2012). Spinal cord gray and white matter, as well as adjacent structures such as ligaments, nerve roots, and blood vessels, are clearly visualized with minimal partial volume effects (Sigmund et al., 2012). Similarly, the first demonstration of 7T fMRI in the spinal cord used a 3D multi-shot protocol with short TE (8 ms) and TR (17 ms), and low flip angles (15°), to minimize geometric distortions and achieve relatively high-resolution images (voxel size = 0.91×0.91×4 mm^3) with an acquisition time of 3.34 sec per volume (278 ms/slice) (Barry et al., 2014). Correlation analyses of low-frequency BOLD fluctuations between gray matter horns revealed resting state spinal cord motor and sensory networks (Barry et al., 2014). The first demonstration of MT acquired quantitative magnetization transfer data via a selective inversion recovery sequence with a turbo field echo readout, and reported the macromolecular to free proton pool size ratio, the MT rate, and R_1 (i.e., $1/T_1$) of the free pool (Dortch et al., 2012). The first demonstration of glutamate CEST used a head coil to examine exchange-related properties of glutamate in gray and white matter in high cervical regions in healthy subjects (Kogan et al., 2013). The first demonstration of amide proton transfer CEST investigated Lorentzian differences between white matter in healthy subjects and both lesions and normal-appearing white matter in patients with multiple sclerosis (Dula et al., 2016b). The first demonstration of ^1H spectroscopy in the spinal cord at 7T used a semi-LASER sequence to quantify N-acetyl aspartate, total choline containing compounds, creatine, and myo-inositol in approximately 7.5 min (effective voxel size = 1 mL, inner volume dimension = 6.4×8.7×18 mm^3) (Henning et al., 2016). This study also used two dipole antennae to excite the spins and provide a more homogeneous B_1^+ field throughout the cord (Henning et al., 2016). Finally, a multi-parametric 7T protocol was recently proposed to perform high-resolution measurements of T_1 and T_2*, and diffusion metrics (radial diffusivity, longitudinal diffusivity, fractional anisotropy, and mean diffusivity), in the cervical cord within a scan time of approximately 30 mins (Massire et al., 2016). This study is the first demonstration of parametric mapping and diffusion imaging in the human spinal cord at 7T, and uses the MNI-Poly-AMU template (Fonov et al., 2014) to facilitate future investigations of clinical biomarkers and reproducibility across 7T sites.

In summary, the 18 abstracts and 21 journal articles listed in Table 1 represent the initial exploration of spinal cord MRI at 7T. All of these publications have considered many or all of the aforementioned technical challenges (e.g., B_0 and B_1 inhomogeneities), so the importance of novel solutions to address the unique challenges of 7T spinal cord MRI cannot be overstated.

CLINICAL APPLICATIONS

A handful of studies have started investigating the benefits of UHF MRI to visualize and quantify spinal cord malformation, injury, or disease. Of the 8 *in vivo* studies that included a patient cohort, 7 presented anatomical (or morphometric) observations and 1 investigated differences in CEST (Dula et al., 2016b). In anatomical imaging, preliminary case studies

confirmed that spinal cord damage due to spinal cord injury (SCI) and amyotrophic lateral sclerosis (Cohen-Adad et al., 2012, 2013) can indeed be visualized at 7T. In patients with multiple sclerosis (MS), ~50% more lesions were detected in the cervical spinal cord at 7T compared to optimized 3T protocols (Dula et al., 2016a; Figure 6), demonstrating the potential of UHF to address the so-called “clinico-radiological paradox” in MS (Barkhof, 2002). A recent abstract has also presented preliminary data in imaging the thoracic cord in MS patients (Lefeuvre et al., 2016). Quantitative imaging via CEST in the cervical cord at 7T also revealed deviations in *z*-spectra between MS patients and healthy volunteers (Dula et al., 2016b). Finally, a preliminary *ex vivo* study presented intriguing data of the entire cord from patients with MS and motor neuron disease (Foxley et al., 2015), introducing the possibility that future longitudinal studies could also correlate 7T *in vivo* images with *ex vivo* imaging and histology post mortem. Overall, these clinical reports are primarily descriptive in nature, and rigorous comparisons between *optimized* 7T and 3T spinal cord protocols will be required for all modalities to better understand the potential clinical benefits of UHF spinal cord imaging.

A specific consideration regarding imaging SCI patients at 7T is that patients who experience an acute injury to the spinal cord often require stabilization hardware (e.g., rods, plates, or screws). Such stabilization hardware is usually metallic, and thus represents a firm contraindication for UHF MRI because the safety of most medical devices and implants is still unknown at field strengths above 3T (Dula et al., 2014; Feng et al., 2015). Therefore, the study of SCI at UHF will, for the foreseeable future, likely be limited in scope to injuries such as cervical spondylotic myelopathy that may not require stabilization hardware or decompressive surgery (Kadaňka et al., 2011).

Clinical applications of UHF spinal cord imaging are still in the early stages, though advances in this area are being supported through parallel UHF non-human primate research. Recent reports in squirrel monkeys at 9.4 Tesla (Wang et al., 2015; Chen et al., 2015) demonstrate how a unilateral dorsal column lesion can model SCI in humans to study changes in spinal cord composition (i.e., quantitative imaging via diffusion tensor imaging, MT, and CEST; Wang et al., 2015) or function (i.e., resting state spinal cord connectivity; Chen et al., 2015). Non-human primate research creates a unique opportunity to study, in a controlled setting, the pathogenesis of SCI and the trajectory of spontaneous recovery after injury. Validated biomarkers of spinal cord integrity or plasticity may be translated back to clinical studies of SCI in humans.

SUMMARY

UHF imaging of the human spinal cord is being pursued by a growing number of research sites worldwide. The predominant challenge in UHF spinal cord imaging is a lack of specialized hardware for imaging the spinal cord at 7T, which is reflected in the fact that more than half of the published reports to date have involved the design and construction of RF coils to image the cord. The next major challenge at 7T is robust B_0 shimming over the spinal cord, which is understandable given its small size and close proximity to large vertebral bones and rapidly changing susceptibility gradients. Imaging at high spatial resolutions will also require novel approaches to data acquisition and processing to mitigate

challenges due to B_0 and B_1 inhomogeneities and shimming, SAR, partial volume effects, motion, and physiological noise. Importantly, our review of the 7T spinal cord literature clearly shows that the research performed to date does not yet reflect the full capabilities of UHF MRI. Although the challenges are both numerous and significant, recent growths in the spinal cord and UHF imaging communities — supported in part by *de novo* spinal cord methods, the influx of 7T systems, and a renewed interest in achieving a more complete understanding of the central nervous system — suggest that a critical mass has been reached in this area of UHF research. Finally, aficionados of UHF MRI are already planning the next generation of UHF systems (Budinger et al., 2016), so spinal cord imaging at 10.5 Tesla or higher will one day become a reality.

Acknowledgments

The authors thank Benjamin N. Conrad for assistance with subject recruitment and scanning, and Laura C. Gee for designing the spine coil montage (Figure 2). This research was supported by the National Institutes of Health (NIH) grants K99EB016689, R00EB016689, and R21NS081437, and the European Union's Horizon 2020 research and innovation programme under the Marie Sklodowska-Curie grant agreement No 659263. The project was also supported by the National Center for Research Resources, grant UL1RR024975-01, which is now at the National Center for Advancing Translational Sciences, grant 2UL1TR000445-06. The content is solely the responsibility of the authors and does not necessarily represent the official views of the NIH.

References

Ali Haghnejad SA, Restivo M, Hoogduin H, Gosselink M, Italiaander M, Mollink J, Raaijmakers A, Klomp DW. Flexible dipoles for multi-transmit head-neck MRI at 7T. Eur Soc Magn Reson Med Biol. 2015; 32:695.

Andreychenko A, Kroeze H, Klomp DWJ, Lagendijk JJW, Luijten PR, van den Berg CAT. Coaxial waveguide for travelling wave MRI at ultrahigh fields. Magn Reson Med. 2013; 70:875–884. [PubMed: 23023780]

Bae KT, Moon CH, Kim JH, Park SH. High-resolution in vivo MR imaging of the human spinal cord at 7 Tesla. Proc Int Soc Magn Reson Med. 2009; 17:633.

Barkhof F. The clinico-radiological paradox in multiple sclerosis revisited. Curr Opin Neurol. 2002; 15:239–245. [PubMed: 12045719]

Barry RL, Rogers BP, Conrad BN, Smith SA, Gore JC. Reproducibility of resting state spinal cord networks in healthy volunteers at 7 Tesla. Neuroimage. 2016; 133:31–40. [PubMed: 26924285]

Barry RL, Smith SA, Dula AN, Gore JC. Resting state functional connectivity in the human spinal cord. Elife. 2014; 3:e02812. [PubMed: 25097248]

Barry RL, Williams JM, Klassen LM, Gallivan JP, Culham JC, Menon RS. Evaluation of preprocessing steps to compensate for magnetic field distortions due to body movements in BOLD fMRI. Magn Reson Imaging. 2010; 28:235–244. [PubMed: 19695810]

Barth M, Breuer F, Koopmans PJ, Norris DG, Poser BA. Simultaneous multislice (SMS) imaging techniques. Magn Reson Med. 2016; 75:63–81. [PubMed: 26308571]

Birn RM, Bandettini PA, Cox RW, Jesmanowicz A, Shaker R. Magnetic field changes in the human brain due to swallowing or speaking. Magn Reson Med. 1998; 40:55–60. [PubMed: 9660553]

Biswal BB, Mennes M, Zuo XN, Gohel S, Kelly C, Smith SM, Beckmann CF, Adelstein JS, Buckner RL, Colcombe S, Dogonowski AM, Ernst M, Fair D, Hampson M, Hoptman MJ, Hyde JS, Kiviniemi VJ, Kötter R, Li SJ, Lin CP, Lowe MJ, Mackay C, Madden DJ, Madsen KH, Margulies DS, Mayberg HS, McMahon K, Monk CS, Mostofsky SH, Nagel BJ, Pekar JJ, Peltier SJ, Petersen SE, Riedl V, Rombouts SARB, Rypma B, Schlaggar BL, Schmidt S, Seidler RD, Siegle GJ, Sorg C, Teng GJ, Veijola J, Villringer A, Walter M, Wang L, Weng XC, Whitfield-Gabrieli S, Williamson P, Windischberger C, Zang YF, Zhang HY, Castellanos FX, Milham MP. Toward discovery science of human brain function. Proc Natl Acad Sci USA. 2010; 107:4734–4739. [PubMed: 20176931]

Biswal B, Yetkin FZ, Haughton VM, Hyde JS. Functional connectivity in the motor cortex of resting human brain using echo-planar MRI. Magn Reson Med. 1995; 34:537–541. [PubMed: 8524021]

Blamire AM, Rothman DL, Nixon T. Dynamic shim updating: a new approach towards optimized whole brain shimming. Magn Reson Med. 1996; 36:159–165. [PubMed: 8795035]

Buckner RL, Krienen FM, Castellanos A, Diaz JC, Yeo BTT. The organization of the human cerebellum estimated by intrinsic functional connectivity. J Neurophysiol. 2011; 106:2322–2345. [PubMed: 21795627]

Budinger TF, Bird MD, Frydman L, Long JR, Mareci TH, Rooney WD, Rosen B, Schenck JF, Schepkin VD, Sherry AD, Sodickson DK, Springer CS, Thulborn KR, Ugurbil K, Wald LL. Toward 20 T magnetic resonance for human brain studies: opportunities for discovery and neuroscience rationale. MAGMA. 2016; 29:617–639. [PubMed: 27194154]

By S, Mojahed E, Barry RL, Smith SA. Multiband excitation enables diffusion tensor imaging of brain stem and cervical spinal cord in clinically feasible scan times at 3T. Proc Int Soc Magn Reson Med. 2016; 24:4405.

Cao Z, Yan X, Grissom WA. Array-compressed parallel transmit pulse design. Magn Reson Med. 2016; 76:1158–1169. [PubMed: 26510117]

Chen LM, Mishra A, Yang PF, Wang F, Gore JC. Injury alters intrinsic functional connectivity within the primate spinal cord. Proc Natl Acad Sci USA. 2015; 112:5991–5996. [PubMed: 25902510]

Cohen-Adad J. Functional magnetic resonance imaging of the spinal cord: current status and future developments. Semin Ultrasound CT MR. 2017; 38:176–186. [PubMed: 28347420]

Cohen-Adad J, Gauthier CJ, Brooks JCW, Slessarev M, Han J, Fisher JA, Rossignol S, Hoge RD. BOLD signal responses to controlled hypercapnia in human spinal cord. Neuroimage. 2010; 50:1074–1084. [PubMed: 20060914]

Cohen-Adad J, Zhao W, Keil B, Ratai EM, Triantafyllou C, Lawson R, Dheel C, Wald LL, Rosen BR, Cudkowicz M, Atassi N. 7-T MRI of the spinal cord can detect lateral corticospinal tract abnormality in amyotrophic lateral sclerosis. Muscle Nerve. 2013; 47:760–762. [PubMed: 23553571]

Cohen-Adad, J., Wheeler-Kingshott, CAM., editors. Quantitative MRI of the spinal cord. London: Elsevier; 2014.

Cohen-Adad J, Zhao W, Wald LL, Oaklander AL. 7T MRI of spinal cord injury. Neurology. 2012; 79:2217. [PubMed: 23183281]

Conrad BN, Lyttle BD, Pawate S, Barry RL, Landman BA, Smith SA. Measuring cross sectional area of the spinal cord at 7T: validating fully automated segmentation. Proc Int Soc Magn Reson Med. 2015; 23:4436.

Curtis AT, Gilbert KM, Klassen LM, Gati JS, Menon RS. Slice-by-slice B_1^+ shimming at 7 T. Magn Reson Med. 2012; 68:1109–1116. [PubMed: 22213531]

de Graaf RA, Brown PB, McIntyre S, Rothman DL, Nixon TW. Dynamic shim updating (DSU) for multislice signal acquisition. Magn Reson Med. 2003; 49:409–416. [PubMed: 12594742]

De Leener B, Kadoury S, Cohen-Adad J. Robust, accurate and fast automatic segmentation of the spinal cord. Neuroimage. 2014; 98:528–536. [PubMed: 24780696]

De Leener B, Lévy S, Dupont SM, Fonov VS, Stikov N, Collins DL, Callot V, Cohen-Adad J. SCT: Spinal Cord Toolbox, an open-source software for processing spinal cord MRI data. Neuroimage. 2017; 145:24–43. [PubMed: 27720818]

Dortch RD, Dula AN, Li K, Hirtle JA, Frame CE, Gaur P, Gore JC, Smith SA. Quantitative magnetization transfer imaging of human cervical spinal cord at 7 Tesla. Proc Int Soc Magn Reson Med. 2012; 20:614.

Duan Q, Duyn JH, Merkle H. Segmented dipole: a remotely reconfigurable near-field dipole antenna transmitter for optimized 7 T spine imaging. Proc Int Soc Magn Reson Med. 2016; 24:3512.

Duan Q, Nair G, Gudino N, de Zwart JA, van Gelderen P, Murphy-Boesch J, Reich DS, Duyn JH, Merkle H. A 7T spine array based on electric dipole transmitters. Magn Reson Med. 2015; 74:1189–1197. [PubMed: 26190585]

Duan Q, Sodickson DK, Lattanzi R, Zhang B, Wiggins GC. Optimizing 7T spine array design through offsetting of transmit and receive elements and quadrature excitation. Proc Int Soc Magn Reson Med. 2010; 18:51.

Duerst Y, Wilm BJ, Dietrich BE, Vannesjo SJ, Barmet C, Schmid T, Brunner DO, Pruessmann KP. Real-time feedback for spatiotemporal field stabilization in MR systems. Magn Reson Med. 2015; 73:884–893. [PubMed: 24634192]

Duerst Y, Wilm BJ, Wyss M, Dietrich BE, Gross S, Schmid T, Brunner DO, Pruessmann KP. Utility of real-time field control in T_2*-weighted head MRI at 7T. Magn Reson Med. 2016; 76:430–439. [PubMed: 26307944]

Dula AN, Pawate S, Dethrage LM, Conrad BN, Dewey BE, Barry RL, Smith SA. Chemical exchange saturation transfer of the cervical spinal cord at 7 T. NMR Biomed. 2016b; 29:1249–1257. [PubMed: 27459342]

Dula AN, Pawate S, Dortch RD, Barry RL, George-Durrett KM, Lyttle BD, Dethrage LM, Gore JC, Smith SA. Magnetic resonance imaging of the cervical spinal cord in multiple sclerosis at 7T. Mult Scler. 2016a; 22:320–328. [PubMed: 26209591]

Dula AN, Virostko J, Shellock FG. Assessment of MRI issues at 7 T for 28 implants and other objects. AJR Am J Roentgenol. 2014; 202:401–405. [PubMed: 24450683]

Duyn JH. The future of ultra-high field MRI and fMRI for study of the human brain. Neuroimage. 2012; 62:1241–1248. [PubMed: 22063093]

Dzyubachyk O, Lelieveldt BPF, Blaas J, Reijnierse M, Webb A, van der Geest RJ. Automated algorithm for reconstruction of the complete spine from multistation 7T MR data. Magn Reson Med. 2013; 69:1777–1786. [PubMed: 22821374]

Edelstein WA, Glover GH, Hardy CJ, Redington RW. The intrinsic signal-to-noise ratio in NMR imaging. Magn Reson Med. 1986; 3:604–618. [PubMed: 3747821]

Eippert F, Kong Y, Jenkinson M, Tracey I, Brooks JCW. Denoising spinal cord fMRI data: approaches to acquisition and analysis. Neuroimage. 2017

Eryaman Y, Guerin B, Keil B, Mareyam A, Herraiz JL, Kosior RK, Martin A, Torrado-Carvajal A, Malpica N, Hernandez-Tamames JA, Schiavi E, Adalsteinsson E, Wald LL. SAR reduction in 7T C-spine imaging using a “dark modes” transmit array strategy. Magn Reson Med. 2015; 73:1533–1539. [PubMed: 24753012]

Feinberg DA, Moeller S, Smith SM, Auerbach E, Ramanna S, Gunther M, Glasser MF, Miller KL, Ugurbil K, Yacoub E. Multiplexed echo planar imaging for sub-second whole brain FMRI and fast diffusion imaging. PLoS ONE. 2010; 5:e15710. [PubMed: 21187930]

Feinberg DA, Setsompop K. Ultra-fast MRI of the human brain with simultaneous multi-slice imaging. J Magn Reson. 2013; 229:90–100. [PubMed: 23473893]

Feng DX, McCauley JP, Morgan-Curtis FK, Salam RA, Pennell DR, Loveless ME, Dula AN. Evaluation of 39 medical implants at 7.0 T. Br J Radiol. 2015; 88 20150633.

Fillmer A, Vannesjo SJ, Pavan M, Scheidegger M, Pruessmann KP, Henning A. Fast iterative pre-emphasis calibration method enabling third-order dynamic shim updated fMRI. Magn Reson Med. 2016; 75:1119–1131. [PubMed: 25950147]

Finsterbusch J. Simultaneous functional MRI acquisition of distributed brain regions with high temporal resolution using a 2D-selective radiofrequency excitation. Magn Reson Med. 2015; 73:683–691. [PubMed: 24574142]

Finsterbusch J. Combined T2*-weighted measurements of the human brain and cervical spinal cord with partial multi-band acceleration. Proc Int Soc Magn Reson Med. 2016; 24:3716.

Finsterbusch J, Eippert F, Büchel C. Single, slice-specific z-shim gradient pulses improve T2*-weighted imaging of the spinal cord. Neuroimage. 2012; 59:2307–2315. [PubMed: 21979381]

Finsterbusch J, Sprenger C, Büchel C. Combined T2*-weighted measurements of the human brain and cervical spinal cord with a dynamic shim update. Neuroimage. 2013; 79:153–161. [PubMed: 23603283]

Fonov VS, Le Troter A, Taso M, De Leener B, Lévêque G, Benhamou M, Sdika M, Benali H, Pradat PF, Collins DL, Callot V, Cohen-Adad J. Framework for integrated MRI average of the spinal cord white and gray matter: the MNI-Poly-AMU template. Neuroimage. 2014; 102(P2):817–827. [PubMed: 25204864]

Foxley S, Mollink J, Ansorge O, Scott C, Jbabdi S, Yates R, De Luca G, Miller K. Whole post-mortem spinal cord imaging with diffusion-weighted steady state free precession at 7T. Proc Int Soc Magn Reson Med. 2015; 23:4429.

Glover GH, Li TQ, Ress D. Image-based method for retrospective correction of physiological motion effects in fMRI: RETROICOR. Magn Reson Med. 2000; 44:162–167. [PubMed: 10893535]

Graessl A, Langner S, Hoehne M, Dieringer MA, Niendorf T. En route to clinical ultrahigh field musculoskeletal MR using multi-purpose transceiver RF modules for spine und shoulder imaging at 7.0 T. Proc Int Soc Magn Reson Med. 2014; 22:1431.

Grams AE, Kraff O, Umutlu L, Maderwald S, Dammann P, Ladd ME, Forsting M, Gizewski ER. MRI of the lumbar spine at 7 Tesla in healthy volunteers and a patient with congenital malformations. Skeletal Radiol. 2012; 41:509–514. [PubMed: 21604210]

Gruetter R. Automatic, localized *in vivo* adjustment of all first- and second-order shim coils. Magn Reson Med. 1993; 29:804–811. [PubMed: 8350724]

Haines K, Smith NB, Webb AG. New high dielectric constant materials for tailoring the B_1^+ distribution at high magnetic fields. J Magn Reson. 2010; 203:323–327. [PubMed: 20122862]

Han H, Song AW, Truong TK. Integrated parallel reception, excitation, and shimming (iPRES). Magn Reson Med. 2013; 70:241–247. [PubMed: 23629974]

Henning A, Koning W, Fuchs A, Raaijmakers A, Bluemink JJ, van den Berg CAT, Boer VO, Klomp DWJ. ^{1}H MRS in the human spinal cord at 7 T using a dielectric waveguide transmitter, RF shimming and a high density receive array. NMR Biomed. 2016; 29:1231–1239. [PubMed: 27191947]

Hock A, MacMillan EL, Fuchs A, Kreis R, Boesiger P, Kollias SS, Henning A. Non-water-suppressed proton MR spectroscopy improves spectral quality in the human spinal cord. Magn Reson Med. 2013; 69:1253–1260. [PubMed: 22745036]

International commission on non-ionizing radiation protection (ICNIRP). Guidelines for limiting exposure to time-varying electric, magnetic and electromagnetic fields (up to 300 GHz). Health Phys. 1998; 74:494–522. [PubMed: 9525427]

Juchem C, Nixon TW, Diduch P, Rothman DL, Starewicz P, de Graaf RA. Dynamic Shimming of the Human Brain at 7 Tesla. Concepts Magn Reson Part B Magn Reson Eng. 2010; 37B:116–128. [PubMed: 20657809]

Juchem C, Nixon TW, McIntyre S, Boer VO, Rothman DL, de Graaf RA. Dynamic multi-coil shimming of the human brain at 7 T. J Magn Reson. 2011; 212:280–288. [PubMed: 21824794]

Kadaňka Z, Bednařík J, Novotný O, Urbánek I, Dušek L. Cervical spondylotic myelopathy: conservative versus surgical treatment after 10 years. Eur Spine J. 2011; 20:1533–1538. [PubMed: 21519928]

Kim DH, Adalsteinsson E, Glover GH, Spielman DM. Regularized higher-order in vivo shimming. Magn Reson Med. 2002; 48:715–722. [PubMed: 12353290]

Koch KM, McIntyre S, Nixon TW, Rothman DL, de Graaf RA. Dynamic shim updating on the human brain. J Magn Reson. 2006; 180:286–296. [PubMed: 16574443]

Kogan F, Singh A, Debrosse C, Haris M, Cai K, Nanga RP, Elliott M, Hariharan H, Reddy R. Imaging of glutamate in the spinal cord using GluCEST. Neuroimage. 2013; 77:262–267. [PubMed: 23583425]

Kong Y, Eippert F, Beckmann CF, Andersson J, Finsterbusch J, Büchel C, Tracey I, Brooks JCW. Intrinsically organized resting state networks in the human spinal cord. Proc Natl Acad Sci USA. 2014; 111:18067–18072. [PubMed: 25472845]

Kraff O, Bitz AK, Kruszona S, Orzada S, Schaefer LC, Theysohn JM, Maderwald S, Ladd ME, Quick HH. An eight-channel phased array RF coil for spine MR imaging at 7 T. Invest Radiol. 2009; 44:734–740. [PubMed: 19809342]

Kraff O, Orzada S, Dammann P, Schlamann M, Ladd ME, Quick HH, Bitz AK. Investigation of 7 Tesla spine MRI with a 5-channel stripline array and an 8-channel loop array. Proc Int Soc Magn Reson Med. 2011; 19:3835.

Krüger G, Glover GH. Physiological noise in oxygenation-sensitive magnetic resonance imaging. Magn Reson Med. 2001; 46:631–637. [PubMed: 11590638]

Krüger G, Kastrup A, Glover GH. Neuroimaging at 1.5 T and 3.0 T: comparison of oxygenation-sensitive magnetic resonance imaging. Magn Reson Med. 2001; 45:595–604. [PubMed: 11283987]

Lakshmanan K, Cloos M, Brown R, Shepherd T, Wiggins GC. A four channel transmit receive "loopole" array for spine imaging at 7.0 Tesla. Proc Int Soc Magn Reson Med. 2015; 23:628.

Larkman DJ, Hajnal JV, Herlihy AH, Coutts GA, Young IR, Ehnholm G. Use of multicoil arrays for separation of signal from multiple slices simultaneously excited. J Magn Reson Imaging. 2001; 13:313–317. [PubMed: 11169840]

Lee G, Jordan C, Tiet P, Ruiz C, McCormick J, Phuong K, Hargreaves B, Conolly S. Improved frequency selective fat suppression in the posterior neck with tissue susceptibility matched pyrolytic graphite foam. J Magn Reson Imaging. 2015; 41:684–693. [PubMed: 24677296]

Lefeuvre J, Duan Q, de Zwart JA, van Gelderen P, Lehericy S, Jacobson S, Reich DS, Nair G. MRI of the thoracic spinal cord in multiple sclerosis at 7T. Proc Int Soc Magn Reson Med. 2016; 24:4397.

Li Y, Xie Z, Pang Y, Vigneron D, Zhang X. ICE decoupling technique for RF coil array designs. Med Phys. 2011; 38:4086–4093. [PubMed: 21859008]

Liu X, Zhou F, Li X, Qian W, Cui J, Zhou IY, Luk KDK, Wu EX, Hu Y. Organization of the intrinsic functional network in the cervical spinal cord: a resting state functional MRI study. Neuroscience. 2016; 336:30–38. [PubMed: 27590264]

Maderwald S, Kraff O, Theysohn JM, Bitz A, Brote I, Wicklow K, Schmitt F, Lazar R, Ladd SC, Quick HH, Ladd ME. Preliminary experience with whole body MRI @ 7T. Proc Int Soc Magn Reson Med. 2008; 16:2716.

Mao W, Smith MB, Collins CM. Exploring the limits of RF shimming for high-field MRI of the human head. Magn Reson Med. 2006; 56:918–922. [PubMed: 16958070]

Massire A, Taso M, Besson P, Guye M, Ranjeva JP, Callot V. High-resolution multi-parametric quantitative magnetic resonance imaging of the human cervical spinal cord at 7T. Neuroimage. 2016; 143:58–69. [PubMed: 27574985]

Moeller S, Yacoub E, Olman CA, Auerbach E, Strupp J, Harel N, Uğurbil K. Multiband multislice GE-EPI at 7 Tesla, with 16-fold acceleration using partial parallel imaging with application to high spatial and temporal whole-brain fMRI. Magn Reson Med. 2010; 63:1144–1153. [PubMed: 20432285]

Nassirpour S, Chang P, Fillmer A, Henning A. A comparison of optimization algorithms for localized in vivo B_0 shimming. Magn Reson Med. 2017

Niendorf T, Sodickson DK, Krombach GA, Schulz-Menger J. Toward cardiovascular MRI at 7 T: clinical needs, technical solutions and research promises. Eur Radiol. 2010; 20:2806–2816. [PubMed: 20676653]

O'Reilly TPA, Webb AG, Brink WM. Practical improvements in the design of high permittivity pads for dielectric shimming in neuroimaging at 7 T. J Magn Reson. 2016; 270:108–114. [PubMed: 27434779]

Padormo F, Beqiri A, Hajnal JV, Malik SJ. Parallel transmission for ultrahigh-field imaging. NMR Biomed. 2016; 29:1145–1161. [PubMed: 25989904]

Pennell DR, Sharma A, Ong HH, Smith SA. B0 fluctuations within the human spinal cord during respiration at 7.0 Tesla. Proc Int Soc Magn Reson Med. 2014; 22:1714.

Raj D, Anderson AW, Gore JC. Respiratory effects in human functional magnetic resonance imaging due to bulk susceptibility changes. Phys Med Biol. 2001; 46:3331–3340. [PubMed: 11768509]

Robitaille PML, Abduljalil AM, Kangarlu A, Zhang X, Yu Y, Burgess R, Bair S, Noa P, Yang L, Zhu H, Palmer B, Jiang Z, Chakeres DM, Spigos D. Human magnetic resonance imaging at 8 T. NMR Biomed. 1998; 11:263–265. [PubMed: 9802467]

San Emeterio Nateras O, Yu F, Muir ER, Bazan C, Franklin CG, Li W, Li J, Lancaster JL, Duong TQ. Intrinsic resting-state functional connectivity in the human spinal cord at 3.0 T. Radiology. 2016; 279:262–268. [PubMed: 26505923]

Schenck JF. The role of magnetic susceptibility in magnetic resonance imaging: MRI magnetic compatibility of the first and second kinds. Med Phys. 1996; 23:815–850. [PubMed: 8798169]

Seifert AC, Dyvorne H, Kim J-w, Zhang B, Xu J. DANTE-EPI for CSF suppression in cervical spinal cord BOLD fMRI at 7T. Proc Int Soc Magn Reson Med. 2016; 24:3720.

Sengupta S, Welch EB, Zhao Y, Foxall D, Starewicz P, Anderson AW, Gore JC, Avison MJ. Dynamic B_0 shimming at 7 T. Magn Reson Imaging. 2011; 29:483–496. [PubMed: 21398062]

Setsompop K, Gagoski BA, Polimeni JR, Witzel T, Wedeen VJ, Wald LL. Blipped-controlled aliasing in parallel imaging for simultaneous multislice echo planar imaging with reduced *g*-factor penalty. Magn Reson Med. 2012; 67:1210–1224. [PubMed: 21858868]

Sigmund EE, Suero GA, Hu C, McGorty K, Sodickson DK, Wiggins GC, Helpern JA. High-resolution human cervical spinal cord imaging at 7 T. NMR Biomed. 2012; 25:891–899. [PubMed: 22183956]

Smith, SA., Dortch, RD., Barry, RL., Gore, JC. Ultra-high field spinal cord imaging. In: Cohen-Adad, J., Wheeler-Kingshott, CAM., editors. Quantitative MRI of the spinal cord. London: Elsevier; 2014. p. 106-119.

Teeuwisse WM, Brink WM, Haines KN, Webb AG. Simulations of high permittivity materials for 7 T neuroimaging and evaluation of a new barium titanate-based dielectric. Magn Reson Med. 2012; 67:912–918. [PubMed: 22287360]

Topfer R, Starewicz P, Lo KM, Metzemaekers K, Jette D, Hetherington HP, Stikov N, Cohen-Adad J. A 24-channel shim array for the human spinal cord: design, evaluation, and application. Magn Reson Med. 2016; 76:1604–1611. [PubMed: 27487798]

Triantafyllou C, Hoge RD, Krueger G, Wiggins CJ, Potthast A, Wiggins GC, Wald LL. Comparison of physiological noise at 1.5 T, 3 T and 7 T and optimization of fMRI acquisition parameters. Neuroimage. 2005; 26:243–250. [PubMed: 15862224]

Triantafyllou C, Hoge RD, Wald LL. Effect of spatial smoothing on physiological noise in high-resolution fMRI. Neuroimage. 2006; 32:551–557. [PubMed: 16815038]

Uğurbil K. The road to functional imaging and ultrahigh fields. Neuroimage. 2012; 62:726–735. [PubMed: 22333670]

van Gelderen P, de Zwart JA, Starewicz P, Hinks RS, Duyn JH. Real time shimming to compensate for respiration induced B_0 fluctuations. Magn Reson Med. 2007; 57:362–368. [PubMed: 17260378]

Vannesjo SJ, Eippert F, Kong Y, Clare S, Miller KL, Tracey I. Breathing-induced B0 field fluctuations in the cervical spinal cord at 7T. Proc Int Soc Magn Reson Med. 2016; 24:49.

Vannesjo SJ, Wilm BJ, Duerst Y, Gross S, Brunner DO, Dietrich BE, Schmid T, Barmet C, Pruessmann KP. Retrospective correction of physiological field fluctuations in high-field brain MRI using concurrent field monitoring. Magn Reson Med. 2015; 73:1833–1843. [PubMed: 24903278]

Vannesjo SJ, Duerst Y, Vionnet L, Dietrich BE, Pavan M, Gross S, Barmet C, Pruessmann KP. Gradient and shim pre-emphasis by inversion of a linear time-invariant system model. Magn Reson Med. 2017

Vaughan JT, Snyder CJ, DelaBarre LJ, Bolan PJ, Tian J, Bolinger L, Adriany G, Andersen P, Strupp J, Ugurbil K. Whole-body imaging at 7T: preliminary results. Magn Reson Med. 2009; 61:244–248. [PubMed: 19097214]

Verma T, Cohen-Adad J. Effect of respiration on the B_0 field in the human spinal cord at 3T. Magn Reson Med. 2014; 72:1629–1636. [PubMed: 24390654]

Versluis MJ, Sutton BP, de Bruin PW, Börnert P, Webb AG, van Osch MJ. Retrospective image correction in the presence of nonlinear temporal magnetic field changes using multichannel navigator echoes. Magn Reson Med. 2012; 68:1836–1845. [PubMed: 22362637]

Vossen M, Teeuwisse W, Reijnierse M, Collins CM, Smith NB, Webb AG. A radiofrequency coil configuration for imaging the human vertebral column at 7 T. J Magn Reson. 2011; 208:291–297. [PubMed: 21134773]

Wang F, Qi HX, Zu Z, Mishra A, Tang C, Gore JC, Chen LM. Multiparametric MRI reveals dynamic changes in molecular signatures of injured spinal cord in monkeys. Magn Reson Med. 2015; 74:1125–1137. [PubMed: 25334025]

Webb AG, Aussenhofer SA. Evaluation of plasma-based transmit coils for magnetic resonance. J Magn Reson. 2015; 261:49–53. [PubMed: 26529202]

Webb AG, Van de Moortele PF. The technological future of 7T MRI hardware. NMR Biomed. 2016; 29:1305–1315. [PubMed: 25974894]

Webb P, Macovski A. Rapid, fully automatic, arbitrary-volume *in vivo* shimming. Magn Reson Med. 1991; 20:113–122. [PubMed: 1943653]

Wheeler-Kingshott CAM, Hickman SJ, Parker GJM, Ciccarelli O, Symms MR, Miller DH, Barker GJ. Investigating cervical spinal cord structure using *axial* diffusion tensor imaging. Neuroimage. 2002; 16:93–102. [PubMed: 11969321]

Wilm BJ, Gamper U, Henning A, Pruessmann KP, Kollias SS, Boesiger P. Diffusion-weighted imaging of the entire spinal cord. NMR Biomed. 2009; 22:174–181. [PubMed: 18727164]

Wilson JL, Jenkinson M, Jezzard P. Optimization of static field homogeneity in human brain using diamagnetic passive shims. Magn Reson Med. 2002; 48:906–914. [PubMed: 12418007]

Wu B, Wang C, Krug R, Kelley DA, Xu D, Pang Y, Banerjee S, Vigneron DB, Nelson SJ, Majumdar S, Zhang X. 7T human spine imaging arrays with adjustable inductive decoupling. IEEE Trans Biomed Eng. 2010; 57:397–403. [PubMed: 19709956]

Xie Z, Zhang X. An 8-channel non-overlapped spinal cord array coil for 7T MR imaging. Proc Int Soc Magn Reson Med. 2008; 16:2974.

Yacoub E, Shmuel A, Pfeuffer J, Van De Moortele PF, Adriany G, Andersen P, Vaughan JT, Merkle H, Ugurbil K, Hu X. Imaging brain function in humans at 7 Tesla. Magn Reson Med. 2001; 45:588–594. [PubMed: 11283986]

Yan X, Cao Z, Grissom WA. Experimental implementation of array-compressed parallel transmission at 7 Tesla. Magn Reson Med. 2016; 75:2545–2552. [PubMed: 27080331]

Yang S, Kim H, Ghim MO, Lee BU, Kim DH. Local in vivo shimming using adaptive passive shim positioning. Magn Reson Imaging. 2011; 29:401–407. [PubMed: 21216551]

Yang QX, Rupprecht S, Luo W, Sica C, Herse Z, Wang J, Cao Z, Vesek J, Lanagan MT, Carluccio G, Ryu YC, Collins CM. Radiofrequency field enhancement with high dielectric constant (HDC) pads in a receive array coil at 3.0T. J Magn Reson Imaging. 2013; 38:435–440. [PubMed: 23293090]

Yu Z, Zhang B, Walczyk J, Chen G, Wiggins G. A 6 channel transmit-receive coil array for 7T cervical spine imaging. Proc Int Soc Magn Reson Med. 2016; 24:2145.

Zhang B, Seifert AC, Kim J-w, Borrello J, Xu J. 7 Tesla 22-channel wrap-around coil array for cervical spinal cord and brainstem imaging. Magn Reson Med. 2017

Zhao W, Cohen-Adad J, Polimeni JR, Keil B, Guerin B, Setsompop K, Serano P, Mareyam A, Hoecht P, Wald LL. Nineteen-channel receive array and four-channel transmit array coil for cervical spinal cord imaging at 7T. Magn Reson Med. 2014; 72:291–300. [PubMed: 23963998]

Zhao Y, Anderson AW, Gore JC. Computer simulation studies of the effects of dynamic shimming on susceptibility artifacts in EPI at high field. J Magn Reson. 2005; 173:10–22. [PubMed: 15705507]

Zheng T, Finnerty M, Yang X, Diprimio M, Beery L, Taylor P, Vannesjo J, Clare S, Fujita H. A cervical spine array coil with volume transmitter at 7 Tesla. Proc Int Soc Magn Reson Med. 2016; 24:2144.

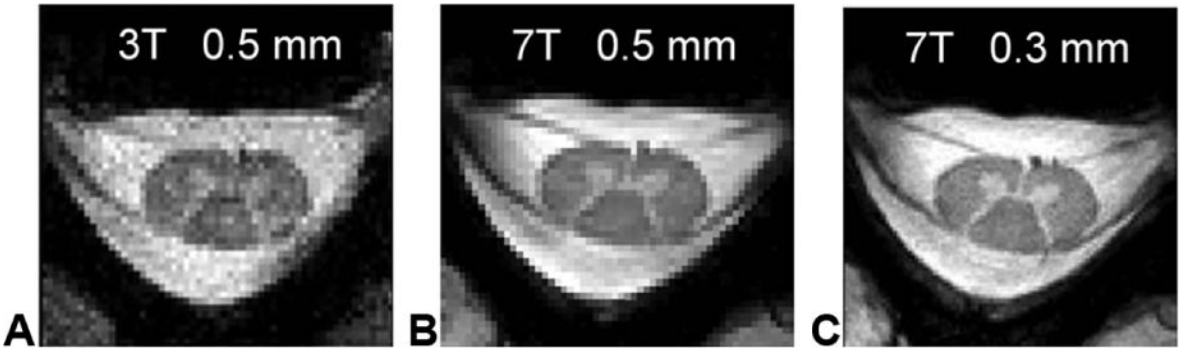

Figure 1.

Comparison of 3T and 7T cervical spinal cord images at C5/C6. (A) 3T image acquired using the 19-channel commercial coil with 0.5 × 0.5 × 3 mm resolution (acquisition time = 1 min 44 sec). (B) 7T image acquired using the 19-channel receive array and four-channel transmit array (Zhao et al., 2014) with 0.5 × 0.5 × 3 mm resolution (acquisition time = 1 min 44 sec). (C) 7T image also acquired using the 19-channel receive array and four-channel transmit array with 0.3 × 0.3 × 3 mm resolution (no interpolation) (acquisition time = 3 min 43 sec). Reproduced from Zhao et al., 2014 with permission from John Wiley and Sons.

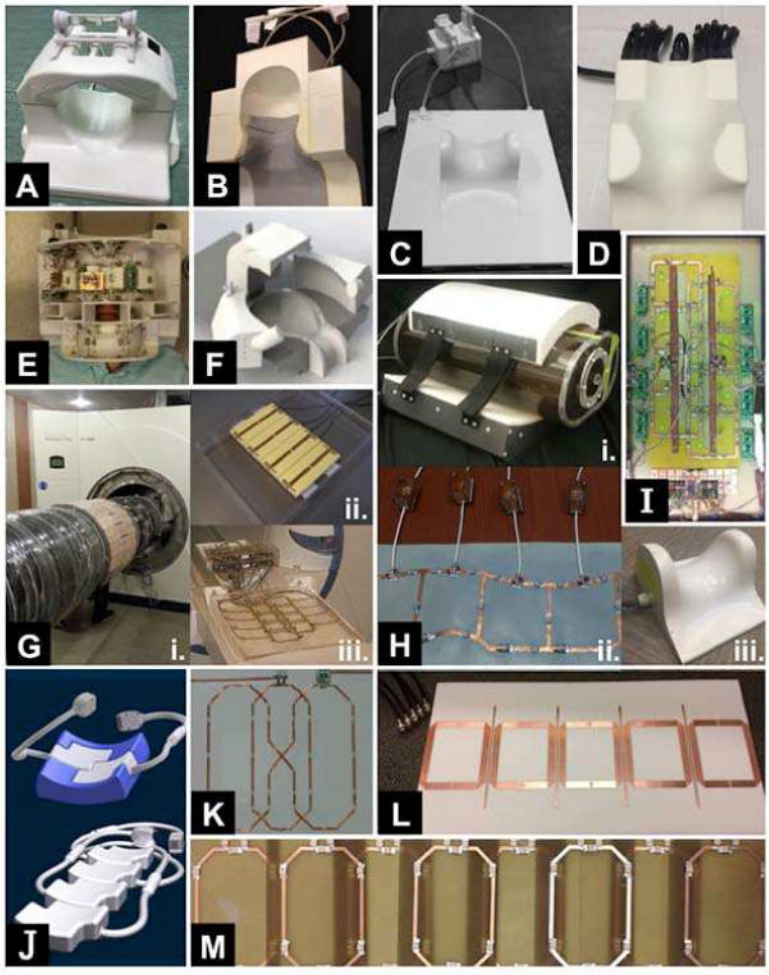

Figure 2.

Montage of coils for human spinal cord MRI at 7T.

(A) Volume transmit and 16-channel receive (manufactured by Quality Electrodynamics) for the cervical cord. Courtesy of Johanna Vannesjo; Oxford Centre for Functional MRI of the Brain, University of Oxford, Oxford, United Kingdom.

(B) Four-channel transmit and 19-channel receive for the cervical cord. Courtesy of Lawrence Wald; Athinoula A. Martinos Center for Biomedical Imaging, Massachusetts General Hospital and Harvard Medical School, Boston, MA, USA.

(C) Eight-channel transceive (manufactured by Rapid Biomedical GmbH) for the cervical cord. Courtesy of Aurélien Massire and Virginie Callot; Center for Magnetic Resonance in Biology and Medicine, Aix-Marseille University, Marseille, France.

(D) Quadrature transmit and 16-channel receive (manufactured by Nova Medical Inc.) for the cervical cord. Courtesy of Samantha By and Seth Smith; Vanderbilt University Institute of Imaging Science, Vanderbilt University Medical Center, Nashville, TN, USA.

(E) Four-channel transmit and 22-channel receive (two panel wrap-around) for the cervical cord and brainstem. Courtesy of Alan Seifert, Bei Zhang, and Junqian Xu; Translational and Molecular Imaging Institute (TMII), Icahn School of Medicine at Mount Sinai, New York, NY, USA.

(F) Flexible 8-channel transmit and 32-channel receive head and cervical spine coil, optimized for x–y and z B_1^+ shimming. Note the full visual clearance and that the setup fits all head sizes. Courtesy of Dennis Klomp et al.; University Medical Center Utrecht and MR Coils, Utrecht, The Netherlands.

(G) (i) Custom-built 32-channel transceive body coil, integrated between bore liner and gradient coil, for the thoracolumbar cord. (ii) Eight-channel flexible transceive body coil, based upon meander stripline elements, for the thoracolumbar cord. (iii) Eight-channel transceive coil, based upon rectangular loop elements, for the cervical cord. All images courtesy of Oliver Kraff and Stephan Orzada; Erwin L. Hahn Institute for Magnetic Resonance Imaging, Essen, Germany.

(H) (i) Four-channel “loopole” transceive for the lumbar cord. (ii) Six-channel flexible transceive for the cervical cord. Both images courtesy of Karthik Lakshmanan; Bernard and Irene Schwartz Center for Biomedical Imaging, New York University School of Medicine, New York, NY, USA. (iii) Four-channel transceive (manufactured by Rapid Biomedical GmbH) for the cervical cord. Courtesy of Eric Sigmund; New York University Langone Medical Center, New York, NY, USA.

(I) Graphical overlay of two electric dipole antennae (transmit) and eight loop coils (receive) for the thoracic cord. Courtesy of Qi Duan, Govind Nair, Natalia Gudino, Jacco A. de Zwart, Peter van Gelderen, Joe Murphy-Boesch, Daniel S. Reich, Jeff H. Duyn, and Hellmut Merkle; National Institute of Neurological Disorders and Stroke, National Institutes of Health, Bethesda, MD, USA.

(J) Modular (top) 8-channel transceive array for the cervical cord and (bottom) 16-channel transceive array for the cervicothoracolumbar cord. Both arrays can be integrated in the patient table cushions and are duly approved by a notified body for implementation in clinical studies. Courtesy of Thoralf Niendorf, MRI.TOOLS GmbH, Berlin, Germany.

(K) Butterfly-shaped coil for the lumbar cord. Two other coils with similar design have been constructed for the cervical and cervicothoracic cords, respectively. Courtesy of Junghwan Kim, Chan-Hong Moon, and Kyongtae T Bae; University of Pittsburgh, Pittsburgh, PA, USA.

(L) Nonoverlapping microstrip transceive array, with induced current compensation or elimination (ICE) or magnetic wall decoupling (Li et al., 2011), for the thoracic cord. Courtesy of Xiaoliang Zhang; University of California, San Francisco; San Francisco, CA, USA.

(M) Quadrature transmit and 8-channel receive for the cervicothoracolumbosacral cord. Courtesy of Andrew Webb; C.J. Gorter Center for High Field Magnetic Resonance Imaging, Leiden, The Netherlands.

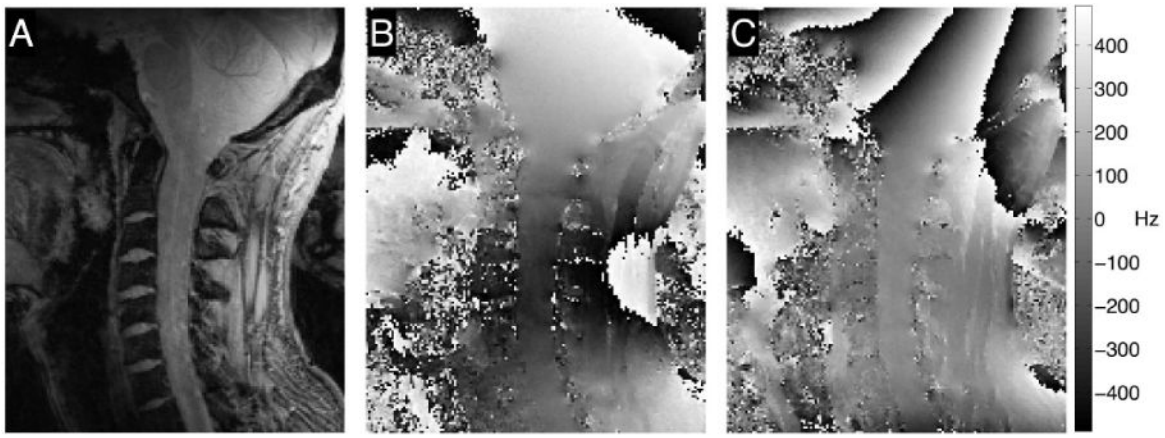

Figure 3.

B_0 shimming over the cervical spinal cord at 7T, using a shim volume covering the spinal cord from C1 to C7. (A) Anatomy of the spinal cord in a healthy volunteer. ΔB_0 field map (13 sagittal slices, in-plane resolution = 1×1 mm^2, slice thickness = 2 mm, TR = 620 ms, first echo time (TE) = 4.08 ms, ΔTE = 1.02 ms, flip angle = 53°) (B) before and (C) after 2^{nd} order B_0 shimming to compensate for magnetic field inhomogeneities within the spinal cord. The shimmed field map reveals residual quasi-periodic high-frequency field distortions along the cord near the intervertebral junctions.

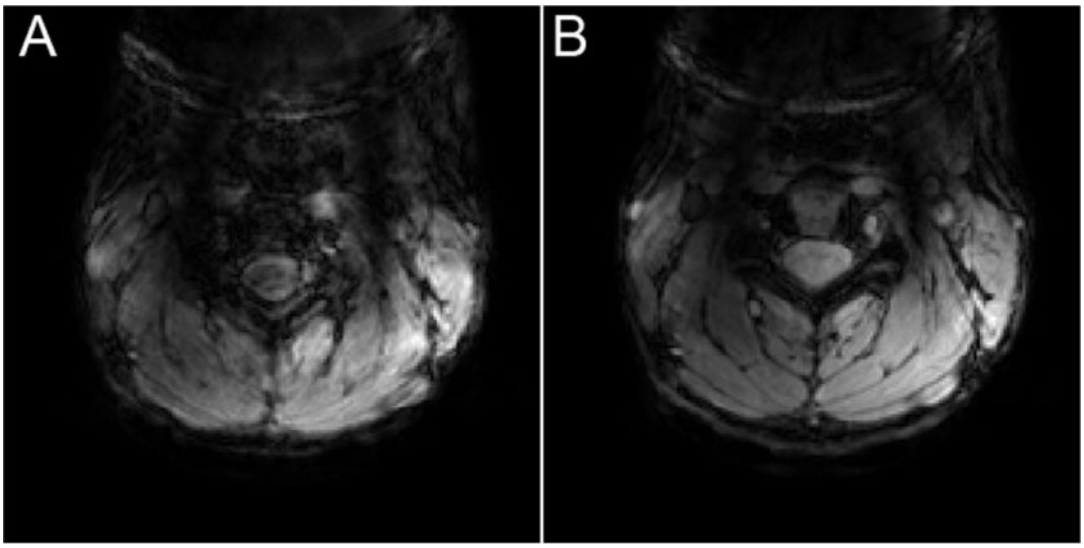

Figure 4.

Challenges of B_0 shimming at 7T. (A) Highly suboptimal automated shimming in the spinal cord at 7T results in unusable functional images. (B) The next run repeats the shimming procedure and achieves a good shim that produces excellent functional images. This extreme variability from one run to the next demonstrates a clear need for more robust spinal cord B_0 shimming at UHF.

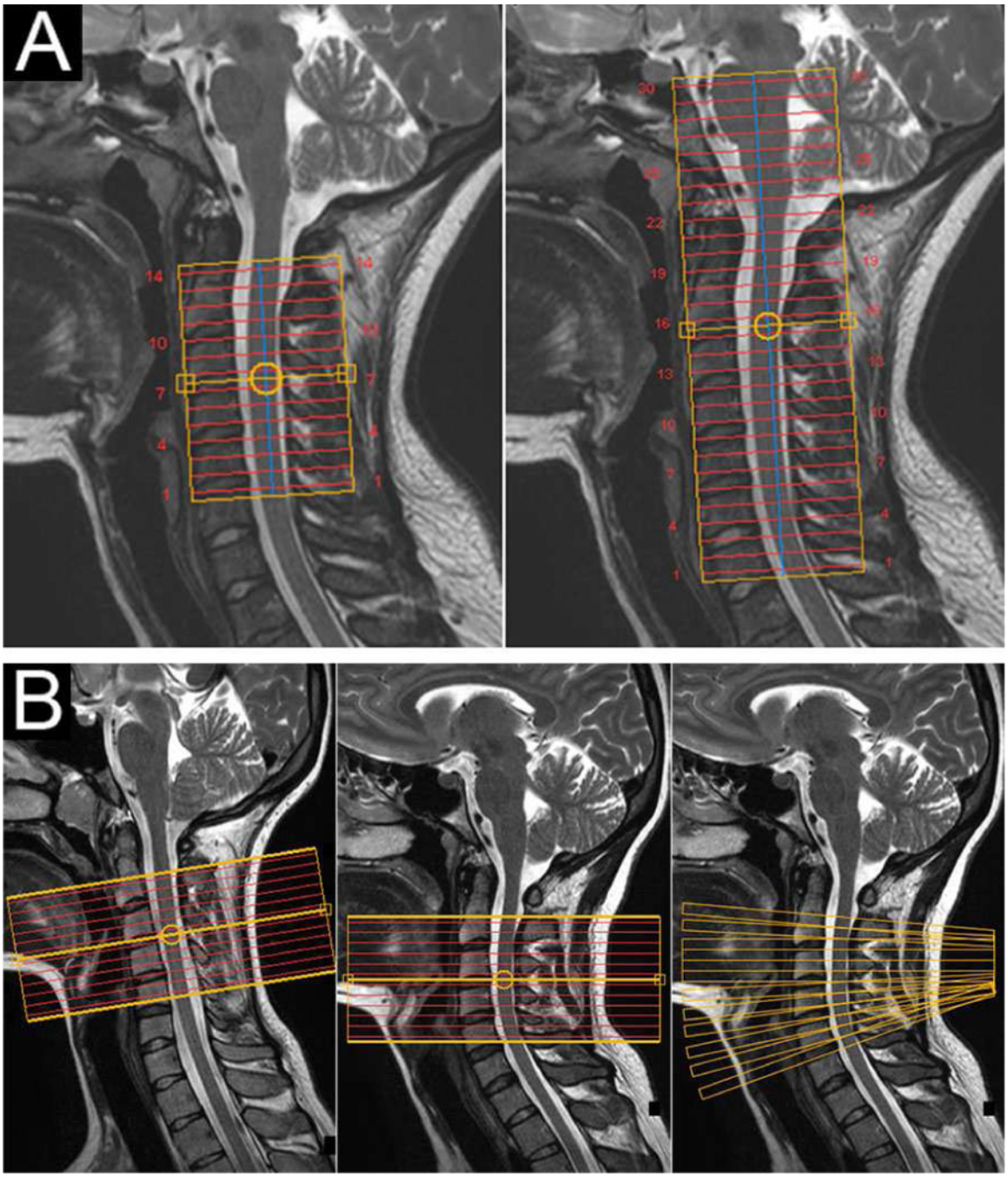

Figure 5.

Improved spinal cord acquisition strategies to be demonstrated at 7T. (A) Diffusion tensor imaging in the cervical spinal cord at 3T. (Left panel) Acquisition without SMS with coverage from C2 to C5. (Right panel) New DTI protocol with SMS illustrating the acquisition of twice as many slices in the same scan time. Note that in the SMS acquisition, the volume placement was raised by one vertebral level (centered on the C2/C3 junction) to cover the brainstem and entire cervical cord. (B) Optimal slice placements along the spinal cord. (Left panel) Placement of 12 5-mm functional slices centered on the C3/C4 junction in

one healthy volunteer. This subject's spinal cord is remarkably straight, which maintains perpendicularity between the slices and the cord and conveniently minimizes through-slice partial volume effects between white and gray matter. (Center panel) The identical placement in another volunteer illustrates curvature at C5 (which is common across subjects), and the challenge of acquiring slices that are consistently perpendicular to a structure that curves. (Right panel) A variable slice angulation scheme that maintains perpendicularity to the spinal cord shown in the center panel would have a variable and optimal angulation for each slice.

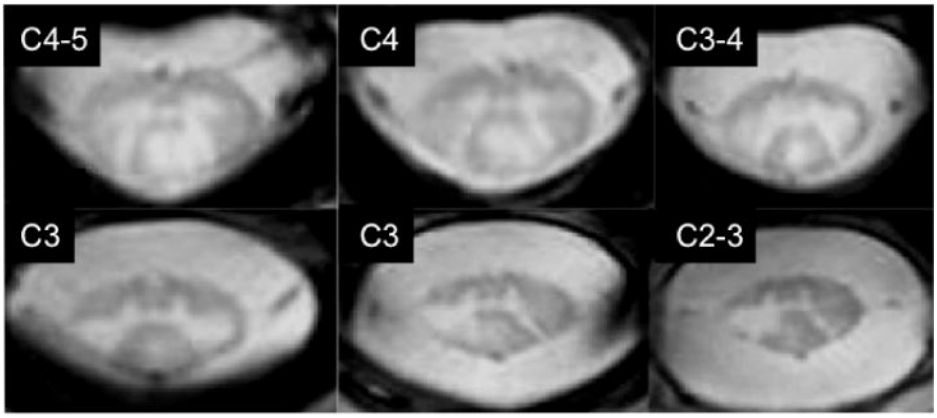

Figure 6.

Visualization of MS lesions is enhanced in T_2*-weighted images at 7T compared to similar T_2*-weighted, or standard-of-care T_2-weighted, acquisitions at 3T (Dula et al., 2016a). Reproduced from Dula et al., 2016a under STM Permissions Guidelines with modifications approved by SAGE Publications Ltd.

Table 1

Publications on spinal cord MRI at 7 Tesla

Topic(s)	Date online[†]	Cohort(s)	Title (abbrev.)	First and last authors	Source	7T vendor	Spine region	Signal detection	Note(s)	Reference
Anatomical imaging	05/05/08	4 healthy volunteers	Preliminary experience with whole body MRI @ 7T	Maderwald S, …, Ladd ME	Proc Int Soc Magn Reson Med	Siemens	Thoracic	34-cm inner-diameter circularly-polarized coil	Conference abstract; not exclusively imaging spine	Maderwald et al., 2008
Coil design	05/05/08	n/a (phantom)	An 8-channel non-overlapped spinal cord array coil…	Xie Z, Zhang X	Proc Int Soc Magn Reson Med	GE	n/a (phantom)	8-channel non-overlapping coil array	Conference abstract; only scanned phantom	Xie & Zhang, 2008
Coil design/Anatomical imaging	05/21/07 // 12/18/08	Healthy volunteer(s)	Whole-body imaging at 7T: preliminary results	Vaughan JT, …, Ugurbil K	Magn Reson Med	Magnex	Thoracolumbar	16-channel transceive coil	Not exclusively imaging spine	Vaughan et al., 2009
Anatomical imaging	04/20/09	3 healthy volunteers	High-resolution in vivo MR imaging of the human sp…	Bae KT, …, Park S-H	Proc Int Soc Magn Reson Med	Siemens	Cervical	butterfly-shaped coil and smaller inner coil to generate quadrature field	Conference abstract	Bae et al., 2009
Coil design	04/20/09 // 08/25/09	10 healthy volunteers	7T human spine imaging arrays with adjustable indu…	Wu B, …, Zhang X	IEEE Trans Biomed Eng	GE	Thoracic	linear array of microstrip transmission line transceive coils		Wu et al., 2010
Coil design/Anatomical imaging	04/20/09 // 10/20/09	1 healthy volunteer and 2 patients with scoliosis	An eight-channel phased array RF coil for spine MR…	Kraff O, …, Quick HH	Invest Radiol	Siemens	Cervico-thoracolumbo-sacral	8-element transceive array		Kraff et al., 2009
Coil design	05/03/10	n/a (phantom)	Optimizing 7T spine array design through offsettin…	Duan Q, …, Wiggins GC	Proc Int Soc Magn Reson Med	Siemens	n/a (phantom)	five coil designs with one, two, or three coils	Conference abstract; only scanned phantom	Duan et al., 2010
Coil design/Anatomical imaging	05/09/11 // 12/04/10	10 healthy volunteers	A radiofrequency coil configuration for imaging th…	Vossen M, …, Webb AG	J Magn Reson	Philips	Cervico thoracolumbo-sacral	quadrature transmit and 8-channel receive		Vossen et al., 2011
Coil design	05/09/11	1 healthy volunteer	Investigation of 7 Tesla spine MRI with a 5-channe…	Kraff O, …, Bitz AK	Proc Int Soc Magn Reson Med	Siemens	Cervical	two transceive coils: 5-channel stripline array and 8-channel loop array		Kraff et al., 2011
Anatomical imaging	05/03/10 // 05/24/11	5 healthy volunteers and 1 patient with spina bifida	MRI of the lumbar spine at 7 Tesla in healthy volu…	Grams AE, …, Gizewski ER	Skeletal Radiol	Siemens	Thoracolumbar	8-channel phased array transceive		Grams et al., 2012
Coil design/Anatomical imaging	05/03/10 // 12/20/11	10 healthy volunteers	High-resolution human cervical	Sigmund EE, …, Helpern JA	NMR Biomed	Siemens	Cervical	4-channel transceive (Rapid Biomedical)		Sigmund et al., 2012

Topic(s)	Date online†	Cohort(s)	Title (abbrev.)	First and last authors	Source	7T vendor	Spine region	Signal detection	Note(s)	Reference
			spinal cord imaging…							
Quantitative magnetization transfer	05/07/12	4 healthy volunteers	Quantitative magnetization transfer imaging of hum…	Dortch RD, …, Smith SA	Proc Int Soc Magn Reson Med	Philips	Cervical	quadrature transmit and 16-channel receive (Nova Medical)	Conference abstract	Dortch et al., 2012
Algorithm validation-image recon.	05/07/12 // 07/20/12	23 healthy volunteers	Automated algorithm for reconstruction of the comp…	Dzyubachyk O, …, van der Geest RJ	Magn Reson Med	Philips	Cervico-thoracolumbo-sacral	10-element linear array		Dzyubachyk et al., 2013
Coil design/Anatomical imaging	05/03/10 // 09/28/12	Healthy volunteers	Coaxial waveguide for travelling wave MRI at ultra…	Andreychenko A, …, van den Berg CAT	Magn Reson Med	Philips	Lumbar	Transmit antenna with coaxial waveguide	Not exclusively imaging spine	Andreychenko et al., 2013
Anatomical imaging	04/22/13 // 11/13/12	1 healthy volunteer and 1 patient with amyotrophic lateral sclerosis	7-T MRI of the spinal cord can detect lateral cort…	Cohen-Adad J, …, Atassi N	Muscle Nerve	Siemens	Cervical	4-channel transmit and 19-channel receive	Case study	Cohen-Adad et al., 2013
Anatomical imaging	04/22/13 // 11/27/12	1 patient with spinal cord injury	7T MRI of spinal cord injury	Cohen-Adad J, …, Oaklander AL	Neurology	Siemens	Cervical	4-channel transmit and 19-channel receive	Case study	Cohen-Adad et al., 2012
Chemical exchange saturation transfer	05/07/12 // 04/09/13	7 healthy volunteers	Imaging of glutamate in the spinal cord using GluC…	Kogan F, …, Reddy R	Neuroimage	Siemens	Cervical	8-channel head coil		Kogan et al., 2013
Coil design/Anatomical imaging	05/07/12 // 08/20/13	2 healthy volunteers	Nineteen-channel receive array and four-channel tr…	Zhao W, …, Wald LL	Magn Reson Med	Siemens	Cervical	4-channel transmit and 19-channel receive		Zhao et al., 2014
Coil design	04/22/13 // 04/18/14	n/a (*In silico*)	SAR reduction in 7T C-spine imaging using a “dark …	Eryaman Y, …, Wald LL	Magn Reson Med	n/a (*In silico*)	n/a (*In silico*)	n/a (simulations of 4-channel loop array with/without “dark” dipole elements)	Simulations	Eryaman et al., 2015
Coil design	05/12/14	4 healthy volunteers	En route to clinical ultrahigh field musculoskelet…	Graessl A, …, Niendorf T	Proc Int Soc Magn Reson Med	Siemens	Cervico-thoracolumbar	16-channel transceive using 4 planar modules	Conference abstract; not exclusively imaging spine	Graessl et al., 2014
B0 field mapping	05/12/14	1 healthy volunteer	B0 fluctuations within the human spinal cord durin…	Pennell DR, …, Smith SA	Proc Int Soc Magn Reson Med	Philips	Cervical	quadrature transmit and 16-channel receive (Nova Medical)	Conference abstract	Pennell et al., 2014
Functional MRI	04/22/13 // 08/05/14	22 healthy volunteers	Resting state functional connectivity in the human…	Barry RL, …, Gore JC	Elife	Philips	Cervical	quadrature transmit and 16-channel receive (Nova Medical)		Barry et al., 2014

Topic(s)	Date online[†]	Cohort(s)	Title (abbrev.)	First and last authors	Source	7T vendor	Spine region	Signal detection	Note(s)	Reference
Coil design/Anatomical imaging	06/01/15	Healthy volunteer(s)	A four channel transmit receive “loophole” array fo…	Lakshmanan K, …, Wiggins GC	Proc Int Soc Magn Reson Med	Siemens	Lumbar	4-channel “loophole” transceive array	Conference abstract	Lakshmanan et al., 2015
Post-mortem diffusion imaging	06/01/15	*Ex vivo*: 2 patients with multiple sclerosis and 1 patient with motor neuron disease	Whole post-mortem spinal cord imaging with diffusi…	Foxley S, …, Miller K	Proc Int Soc Magn Reson Med	Siemens	Cervico-thoracolumbo-sacral	24-channel coil (Quality Electrodynamics) and 16-channel coil (Rapid Biomedical)	Conference abstract	Foxley et al., 2015
Algorithm validation-image segmentation	06/01/15	18 healthy volunteers and 20 patients with multiple sclerosis	Measuring cross sectional area of the spinal cord …	Conrad BN, …, Smith SA	Proc Int Soc Magn Reson Med	Philips	Cervical	quadrature transmit and 16-channel receive (Nova Medical)	Conference abstract	Conrad et al., 2015
Coil design/Anatomical imaging	05/12/14 // 07/20/15	2 healthy volunteers	A 7T spine array based on electric dipole transmit…	Duan Q, …, Merkle H	Magn Reson Med	Siemens	Thoracic	Transmit: two electric dipole antennae; Receive: 8 loop coils		Duan et al., 2015
Anatomical imaging	06/01/15 // 07/24/15	13 healthy volunteers and 15 patients with multiple sclerosis	Magnetic resonance imaging of the cervical spinal …	Dula AN, …, Smith SA	Mult Scler	Philips	Cervical	quadrature transmit and 16-channel receive (Nova Medical)		Dula et al., 2016a
Coil design/Anatomical imaging	10/01/15	Healthy volunteer(s)	Flexible dipoles for multi-transmit head-neck MRI …	Ali Haghnejad SA, …, Klomp DW	Eur Soc Magn Reson Med Biol	Philips	Head + Cervical	Transmit: eight flexible dipole antennae; Receive: 32-channel array	Conference abstract	Ali Haghnejad et al., 2015
Functional MRI	06/01/15 // 02/26/16	23 healthy volunteers	Reproducibility of resting state spinal cord netwo…	Barry RL, …, Gore JC	Neuroimage	Philips	Cervical	quadrature transmit and 16-channel receive (Nova Medical)		Barry et al., 2016
B0 field mapping	05/09/16	2 healthy volunteers	Breathing-induced B0 field fluctuations in the cer…	Vannesjo SJ, …, Tracey I	Proc Int Soc Magn Reson Med	Siemens	Cervical	volume transmit and 16-channel receive (Quality Electrodynamics)	Conference abstract	Vannesjo et al., 2016
Coil design	05/09/16	1 healthy volunteer	A cervical spine array coil with volume transmitte…	Zheng T, …, Fujita H	Proc Int Soc Magn Reson Med	Siemens	Cervical	volume transmit and 16-channel receive (Quality Electrodynamics)	Conference abstract	Zheng et al., 2016
Coil design	05/09/16	Healthy volunteer(s)	A 6 channel transmit-receive coil array for 7T cer…	Yu Z, …, Wiggins G	Proc Int Soc Magn Reson Med	Siemens	Cervical	6-channel transceive	Conference abstract	Yu et al., 2016
Coil design	05/09/16	n/a (phantom)	Segmented dipole: a remotely reconfigurable near-f…	Duan Q, …, Merkle H	Proc Int Soc Magn Reson Med	Siemens	n/a (phantom)	segmented dipole antenna	Conference abstract	Duan et al., 2016

Topic(s)	Date online[†]	Cohort(s)	Title (abbrev.)	First and last authors	Source	7T vendor	Spine region	Signal detection	Note(s)	Reference
Functional MRI	05/09/16	1 healthy volunteer	DANTE-EPI for CSF suppression in cervical spinal c…	Seifert AC, …, Xu J	Proc Int Soc Magn Reson Med	Siemens	Cervical	4-channel transmit and 22-channel receive	Conference abstract	Seifert et al., 2016
Anatomical imaging	05/09/16	1 healthy volunteer and 2 patients with multiple sclerosis	MRI of the thoracic spinal cord in multiple sclero…	Lefeuvre J, …, Nair G	Proc Int Soc Magn Reson Med	Siemens	Thoracic	Transmit: two electric dipole antennae; Receive: 8 loop coils	Conference abstract	Lefeuvre et al., 2016
Coil design/Spectroscopy	05/07/12 // 05/18/16	3 healthy volunteers	1H MRS in the human spinal cord at 7T using a diel…	Henning A, …, Klomp DWJ	NMR Biomed	Philips	Cervical	Transmit: two dipole antennae attached to a neck pillow filled with D2O; Receive: 30-channel array		Henning et al., 2016
Chemical exchange saturation transfer	05/07/12 // 07/26/16	10 healthy volunteers and 10 patients with multiple sclerosis	Chemical exchange saturation transfer of the cervi…	Dula AN, …, Smith SA	NMR Biomed	Philips	Cervical	quadrature transmit and 16-channel receive (Nova Medical)		Dula et al., 2016b
Diffusion/Parametric mapping (T1, T2, T2*)	05/09/16 // 08/26/16	10 healthy volunteers	High-resolution multi-parametric quantitative magn…	Massire A, …, Callot V	Neuroimage	Siemens	Cervical	8-channel transceive (Rapid Biomedical)		Massire et al., 2016
Coil design/Anatomical imaging/ Functional MRI/Diffusion	06/01/15 // 11/17/16	2 healthy volunteers	7 Tesla 22-channel wrap-around coil array for cerv…	Zhang B, …, Xu J	Magn Reson Med	Siemens	Cervical	22-channel coil with 4 transceive elements and 18 receive-only elements		Zhang et al., 2017

[†]The first date refers to initial presentation of the research as an abstract. A second date, if present, refers to the day that research was published online in a peer-reviewed journal. Rows are sorted in chronological order where date of journal publication supersedes date of conference presentation.